UNIVERSITY OF CALIFORNIA SAN DIEGO

Modeling the Influence of ASD Risk Genes on Cortical Connectivity in Forebrain Patterned Assembloids

A Thesis submitted in partial satisfaction of the requirements for the degree Master of Science

in

Biology

by

Thomas Joseph Maxwell Kuret

Committee in charge:

Professor Fred Gage, Chair
Professor Nicholas Spitzer, Co-Chair
Professor William McGinnis
Professor Yimin Zou

2020

The Thesis of Thomas Joseph Maxwell Kuret is approved, and it is acceptable in quality and form for publication on microfilm and electronically:

_____

_____

_____

Co-Chair

_____

Chair

University of California San Diego

2020

DEDICATION

This thesis is dedicated to my loving family – my parents, sister and grandparents – without whom my accomplishments in science would be impossible.

Today, I have carried Madame Zeroni up the mountain.

EPIGRAPH

There is hope in dreams, imagination, and in the courage of those who wish to make those dreams a reality

Jonas Salk

TABLE OF CONTENTS

LIST OF FIGURES

LIST OF TABLES

ACKNOWLEDGEMENTS

I would like to thank Dr. Rusty Gage and Dr. Simon Schafer, for their constant support and mentorship throughout the completion of this project. Membership in The Gage Lab has been an exciting opportunity and a privilege.

I would also like to acknowledge the numerous, knowledgeable staff throughout the Salk Institute. Without the insight and aid from Gage Lab Members, The Stem Cell Core Facility, The Biophotonics Core Facility and Facility Services, this project would not be possible.

I would like to thank Dr. Tong Zhang and Sammy Weiser-Novak, M.S. for applying their microscopy expertise and patience to this project. Both were consistently available to troubleshoot, fix, and when in doubt, unplug any difficult equipment.

I would also like to thank Dr. Shani Stern for lending her knowledge and time to complete the electrophysiology component of this project and providing good company while doing it.

Finally, the knowledge of Ken Diffenderfer, M.S. and Aimee Pankonin, B.S., Monique Schafer, B.S., and Sarah Fernandes, M.S. was instrumental in accomplishing the complex tissue culture goals for this project, and making long nights in tissue culture something to look forward to, rather than something to dread.

Thank you to all who influenced and guided this project, and the many friendships that were formed along the way.

ABSTRACT OF THE THESIS

Modeling the Influence of ASD Risk Genes on Cortical Connectivity in Forebrain Patterned Assembloids

by

Thomas Joseph Maxwell Kuret

Master of Science in Biology

University of California San Diego, 2020

Professor Fred Gage, Chair
Professor Nicholas Spitzer, Co-Chair

Autism spectrum disorder (ASD) is a multifactorial disease, suspected to originate during early fetal cortical development. Due to its symptomology and complex genetic etiology, developmental studies of autism largely rely on analysis of postmortem tissue. Recently, cortical organoids have impacted ASD research by providing highly organized tissue models that recapitulate early fetal human development. Here, forebrain cortical organoids (FBOs) derived from human induced pluripotent stem cells (iPSCs) are employed in a novel assembloid technique to model the basic organization principles of the cortical

connectome. In vitro fusion of two FBOs results in a single assembloid unit that demonstrates key developmental processes: axon fasciculation and pathfinding. Characterization of the assembloid system was performed using immunohistochemistry and identified fascicules (“tracts”) which projected into the adjacent cortical unit and strongly correlated with an axonal identity. Additionally, electrophysiological recordings and correlative electron microscopy provide evidence of functional activity and reciprocal connectivity between assembloid “hemispheres”. Using the assembloid model, knock down of two high confidence ASD risk genes was assessed. Live cell imaging was used to capture short-term (seven days) and long-term changes (six weeks) in axon tracts. Findings from the project demonstrated that disruption of *Contactin-associated protein-like 2* (CNTNAP2, Caspr2) or *immunoglobulin superfamily containing leucine-rich repeat 2* (ISLR2, Linx) impact axon pathfinding and fasciculation. Knock down of CNTNAP2 resulted in absence of axon tracts during the early developmental timepoint, while knock down of ISLR2 resulted in a loss of fasciculation but not outgrowth, at both time points assayed. These findings elucidate the role of two key ASD risk genes during development and their putative impact on human cortical connectivity.

INTRODUCTION

Autism Spectrum Disorder (ASD) is a prominent disease with both syndromic and idiopathic pathologies. CDC Estimates of ASD prevalence are 1:59 children, with an approximate collective cost of $11.5-$60.9 billion USD per annum. Additionally, individuals with ASD accrue an additional medical cost of $4,110-$6,200 per annum[1]. Considering the high economic and social cost of ASD, early diagnostic methods and treatments stand to significantly benefit the population. ASD is defined by core symptomologies: repetitive behaviors and social and communicatory deficits; however, significant heterogeneity in symptomology, severity, and risk exist within the spectrum.

Impaired balance of long-range and short-range connectivity is thought to be associated with mental disorders such as autism[2]; however, most morphological studies rely on postmortem tissue from patients, obfuscating the developmental timeline of ASD. Cause of death or contraindicating health conditions can impact postmortem tissue quality and obscure ASD-specific pathology. Finally, postmortem tissue is mostly limited to late stage disease pathogenesis, preventing observation of early development. As a result, efforts to identify developmental events and processes involved in ASD pathogenesis have been ambiguous. A prominent research initiative is the Simons Foundation Autism Research Initiative (SFARI). SFARI aggregates peer-reviewed literature on ASD studies, and generates a database of genes suspect to contributed to ASD[3]. Previous studies have linked CNTNAP2 with both syndromic[4] and idiopathic forms of the disorder[5,6]. In addition to single genes, new advances in biotechnology have identified gene networks and pathways implicated in ASD pathogenesis[7,8]. This new perspective has revealed gene candidates

previously obscured - a study by Schafer et al. 2019[9] identified a series of highly connected, regulatory gene networks implicated in ASD. Based on this study, we investigated ISLR2 as another risk gene. We aimed to better characterize how both gene candidates contribute to the developmental timeline and pathology of ASD. Current studies have elucidated functions of both ISLR2 and CNTNAP2, but are limited in time scope, species, or complexity. We propose a novel model system of Cortical Organoid Assembloids (COA) to complement current research and to provide a high-resolution model for recapitulating specific aspects of early human brain development and their relation to ASD.

CNTNAP2 encodes for Caspr2, a member of the neurexin super family and a highly conserved protein with several known receptor-ligand interaction domains, suggesting a prominent role in cell-cell signaling and nervous system development[10]. Early work demonstrated the role of Caspr2 in organizing and localizing potassium channels during later development[11]; however, recent studies have also revealed high expression during fetal development, suggesting CNTNAP2 also plays an early role in development. Morphological studies have shown that loss of CNTNAP2 results in decreased dendritic arborization and synaptic transmission, without impacting action potential wave form, during early development of primary cultured mouse cortical neurons [12]. Additional work by Peñagarikano et al. 2011 revealed migration abnormalities via the presence of ectopic Cux1+ neurons in deep cortical layers and epileptic network activity, in CNTNAP2 null mice[13]. CNTNAP2 loss has also been connected to a reduction in long-range cortical connectivity and impaired cortical integration[14]. These studies suggest CNTNAP2 plays a crucial role in promoting axon outgrowth and connectivity in the developing cortex and that impaired CNTNAP2 expression recapitulates several known ASD pathologies.

By contrast, ISLR2 is not as well documented. Work by Panza et al. 2015 identified the protein structure of ISLR2 as containing a leucine-rich repeat sequence – a sequence also present in the slit-robo pathway involved in axon guidance and other regulatory processes[15]. A study by Abudureyimu et al. 2018 documented its essential role in the formation of the anterior commissure[16]. Mice with heterozygous loss of ISLR2 resulted in aberrant projection of thalamocortical axons, while homozygous loss caused perinatal death. Using primary culture, the group also established the role of ISLR2 in cytoskeletal regulation and demonstrated impaired neurite extension – reinforcing the role of ISLR2 in axon pathfinding. Another primary culture study by Mandai et al. 2014 confirmed the need for ISLR2 in axon pathfinding and corticothalamic integration[17]. While these features have been associated with ASD pathology, few studies have investigated this link.

While these studies have documented functions of both CNTNAP2 and ISLR2, several barriers to further research need to be addressed. Primarily, ASD is rooted in high order cortical function and the unique social complexity of humans. These facets are difficult to recapitulate in current model systems – while CNTNAP2 expression is enriched in human frontal cortical areas, mice do not display a similar enrichment[18]. Indeed, CNTNAP2 expression has be suggested to correlate with the evolution of complex social behaviors in humans and other primates. The discovery of induced pluripotent stem cell (hiPSC) technologies is one solution for human disease modeling. Human iPSC models can be used to recapitulate early aspects of development in a dish through monolayer systems, to complement animal models.

However, ASD pathologies suggest a deep malfunction in intercortical connectivity, which cannot be reproduced in 2D neuronal cultures. While new cerebral organoid technologies offer highly organized model systems, they are restricted to modeling local

circuitry and connectivity. The diversity of these model systems has created a fractured landscape. Recently, a new advancement in organoid culture techniques has allowed researchers to model interactions of different brain regions. This new perspective stands to further advance existing assembloid models to generate a platform for assessing intracortical short and long-range connectivity. We use this new platform to further investigate the roles of CNTANP2 and ISLR2 in cortical connectivity. Specifically, we seek to define key developmental processes and abnormalities in inter-cortical connectivity, induced by the knock down of CNTNAP2 or ISLR2.

RESULTS

Generation of Cortical Organoid Assembloids (COAs) as a Model for Reciprocal Cortical Connectivity

The generation of forebrain-specific organoids (FBOs) was based on a guided approach[19] that allows for recapitulation of early corticogenesis. Briefly, dual SMAD inhibition[20] (see methods) was performed to drive early ectodermal fate and subsequent activation of Wnt signaling to generate dorsal forebrain (Fig. 1a).

Using immunofluorescence (IF) and retroviral birth-dating, we determined 28 days in vitro (DIV) to coincide with the onset of neurogenesis and the appearance of CTIP2+ excitatory neurons that form cortical-plate-like regions in these organoid models. GFP-expressing retrovirus was administered at this timepoint to selectively label dividing radial glia-like cells in the ventricular-like zones of developing FBOs, and confirmed that the progenies of these cells give rise to the neuronal population with the majority expressing the deep layer markers CTIP2 6 weeks post infection (6wpi – Figure 1b). GFP+/CTIP2+ neurons exhibited a complex dendritic arborization and integrated into the cortical plate-like (CP) structure that emerged around a ventricular zone-like (VZ) region. We sought to characterize the local connectivity within single FBOs, using the g-deleted rabies system[21] (Figure 1c). We infected FBOs using hSyn::HTB-GFP (Addgene # 30195) that expresses both the rabies glycoprotein and TVA receptor, under the control of the human synapsin promoter. This restricted the starter infection to mature neurons. Four weeks after infection, G-deleted rabies virus (Addgene # 32636) was administered to allow infection of the starter cells. Only starter cells express the G-protein, and as a result are double labeled with GFP and

mCherry. By expressing the glycoprotein, starter neurons infected by both viruses allow the rabies virus to transynaptically label presynaptic neurons. FBOs displayed both starter (GFP+/mCherry+) and presynaptic neurons (mCherry+/GFP-) locally (Figure 1c), suggesting the presence of local interconnected neuronal circuits.

The human cortex is a remarkably complex structure and connectivity constitutes one of its basic organizational principles. Cortical excitatory neurons contribute to the integration and segregation of regional connectivity during development, through balancing short and long-range connections[2,22]. To model long-range connections between different cortical units (Fig 2a), we established an assembloid system by fusing FBOs that ubiquitously expressed GFP (GFP+, starter organoid) with unlabeled FBOs (GFP-, target organoid). These cortical organoid assembloids (COAs) were generated from two FBO units at 28 days in vitro (DIV) (Figure 2b), which were fused along the cortical plate to prevent cell body migration between assembloid “hemispheres”. Notably, COA units demonstrated a high level of interconnectivity, with GFP+ projections robustly extending into cortical regions of the target organoid (Figure 2c). These projections demonstrated a high degree of colocalization with the marker smi312, a mixture of monoclonal antibodies that reacts against axonal neurofilaments (Figure 2c,d), suggesting that the GFP+ projections observed are indeed axons originating from the starter FBO. Additionally, GFP+ projections were primarily found in superficial regions of the target organoid (Figure 3a). Regional projection patterns of GFP+ axons were assessed in the target organoid by co-staining with MAP2, a pan neuronal marker. Interestingly, axonal projections were consistently found only in MAP2+ CP-like regions (Figure 3b,c). Together, these data suggested that COAs establish axonal projections onto neuronal targets in an organized fashion, rendering them a suitable model for studying cortico-cortical projections.

Characterization of Long-Range Connectivity in Cortical Organoid Assembloids

To further characterize local and long-range connectivity in our COA system, we employed the monosynaptic rabies tracer system (RV-dG) as indicated above. This system achieves monosynaptic, retrograde circuit tracing by substituting the glycoprotein from the rabies genome with the coding sequence for mCherry. Initial infection of a single FBO unit with a helper lentivirus expressing the TVA receptor, the rabies glycoprotein and GFP under the human synapsin promoter, enabled specific targeting of the mature neuronal population. Here, the starter organoid was infected using a lentivirus expressing the TVA receptor, the rabies glycoprotein and GFP under the human synapsin promoter prior to assembly, thereby restricting the neuronal starter population to a single hemisphere of the COA. Following fusion to an un-transfected FBO unit, assembloids were further matured for 8 weeks to allow for axon growth and synaptic targeting. EnVA-pseudotyped rabies (RV-dG CAG::mCherry) was then used to infect the COA 8 weeks post assembly (wpa) to target the hSyn::HTB-GFP expressing neuronal population in the starter hemisphere (Figure 4a and b) Histological assessment of showed that the starter HTB-GFP expressing neuronal starter population was confined to a single hemisphere (Figure 4c). In line with our previous observations, local neuronal connections were present in the starter organoid as indicated by the presence of both mCherry+/GFP- and double labeled neurons (Figure 4c,d). Strikingly, the target cortical organoid unit only contained mCherry+/GFP- neurons while no starter neuron was observed (Figure 4e)., Taken together, these experiments demonstrate the presence of both local and long-range cortico-cortical connections within our COA system.

To further investigate synapse formation with long-range targets, we performed electron microscopy and correlative array tomography immuno-fluorescence on our COA

system. Three regions of interest in ultimate proximity to GFP+ axon fibers present in the target organoid were micro-dissected (Figure 5a). Arrays of 70nm serial sections were stained for GFP in order to identify the invading axon fibers from the GFP-expressing starter organoid (Figure 5b,c). Overview imaging of the array revealed intact cellular membranes and quality tissue preservation (Figure 5d). High resolution scanning electron microscopy imaging of regions fibers detected in the array yielded a putative synapse (Figure 5d). Further analysis is currently performed to validate synaptic integrity and target specificity, including correlative analysis between PSD95, synapsin and GFP+. While qualitative scanning electron microscopy identified suggested the presence of synaptic structures, further analysis is required to assess synaptic maturity and specificity to target neurons.

Cortical Assembloids show functional neuronal activity

Given the formation of interhemispheric axonal projections and the presence of synapses, we next sought to investigate whether the neuronal populations that contribute to the observed interhemispheric connectivity are indeed electrophysiologically functional. For this, slice preparations of COAs were prepared in order to perform electrophysiological recordings of evoked extracellular current and field potentials. The COA slice cultures were stimulated with an electrode placed on the starter hemisphere (Figure 6a). A 3V symmetrical pulse with 10 ms duration was chosen to strongly induce activity proximal to the stimulating electrode. When the recording electrode was placed inside the starter organoid, a field current of 226.4 pA was detected with an 89.29 ms latency (Figure 6b). When the recording electrode was moved to a distal region of the connected target organoid in proximity to GFP+ projections, the resulting field currents showed a lower amplitude and higher latency: -136.1 pA, 100.59 ms (Figure 6c). Together these data indicate that functional field currents can be

evoked in COAs and further propagated into the connected target organoid. Further paired-single cell patch-clamp recordings are warranted to confirm functional synaptic connectivity between distant interconnected neurons.

Assessing the functional implications of ASD-associated genes on cortical neuron development

CNTNAP2 is a high risk ASD susceptibility gene, with implications in axon outgrowth. ISLR2 on the other hand is a suspected risk gene in ASD, involved in axon routing. To assess the functional implications of these genes on human cortical development, we designed shRNAs specifically targeting the coding sequence of the genes (Fig. 7a,b). As mutations associated with ASD are in the majority of cases heterozygous, we aimed to investigate the gene-specific implications following moderate knock down, rather than inducing a complete loss-of-function. This allowed us to capture a more disease-relevant scenario.

Knock down efficiencies of multiple shRNAs targeting either CNTNAP2 or ISLR2 were assessed in neuronal monolayer cultures. Therefore, human iPSC-derived neural progenitor cells were electroporated with plasmids containing the respective shRNAs. Electroporated cultures were puromycin selected and processed for qPCR analysis of gene expression. Compared to those cultures expressing a non-target-control (NTC shRNA), two of the tested shRNAs against CNTNAP2 resulted in a significant reduction of CNTNAP2 gene expression, down to 30% ($P = 0.0001$, two tailed t-test, Figure 7c). Since ISLR2 expression increases later in development, we determined the knock down efficiency of the ISLR2-targeting shRNAs in 28 DIV FBO cultures. ISLR2 knock down in FBOs stably

expressing ISLR2-targeting shRNAs resulted in a 50%-decrease in target gene expression, but not housekeeping genes such as GAPDH (P = 0.0110, two tailed t-test, Figure 7d).

To assess the implications of CNTNAP2 and ISLR2 on cortical neuron development, we used retroviruses constitutively expressing GFP and one of the shRNAs targeting either CNTNAP2 or ISLR2. A non-targeting shRNA (NTC) was used as control. To target dividing radial glia-like cells in VZ-like regions, retrovirus was administered at 28DIV as described above and FBOs were harvested 4 weeks post infection (wpi). (Figure 8a). Regions containing clear CP and VZ areas were imaged using confocal microscopy, and individual neurons were reconstructed using the software Neurolucida[23] (Figure 8b). Sholl analysis (radius increments 5μm) of reconstructed neurons revealed no significant difference in overall morphology or complexity between conditions (Figure 8c,d). To assess deficiencies in the migratory process of early born cortical neurons, we determined the relative position of GFP+/CTIP2+ cells. Migration was defined as absolute distance that a neuron had traveled from the VZ. Interestingly, neurons deficient for ISLR2 showed migratory impairments as compared with controls, whereas no significant difference was observed in those neurons deficient for CNTNAP2 (ISLR2 vs NTC; n=79, P <0.0001, Mann-Whitney test (Figure 8e).

Assessing the functional implications of ASD-associated genes on long-range cortical connectivity

Disturbance of the balance of long-range and short-range connections are thought to be associated with disorders such as ASD. To allow prolonged organoid culture as well as easy accessibility for live imaging, we established a COA slice culture system.

Simple brightfield imaging of COA slice cultures showed intact VZ-like and CP-like areas following vibratome sectioning (Figure 9a). Additionally, COA slice cultures enables long term culture up to a stage when later-born SATB2+ emerge (Figure 9b). Suspending the slice culture inserts in a glass bottom imaging dish (Cellvis #D35-20-1.5-N) allowed us to perform longitudinal imaging of COA slices (Figure 9c). Individually acquired images can be overlaid to generate a time series, allowing for the movement of axon fascicules and fibers to be tracked (Figure 9d).

COA slice cultures were imaged every 48 hours, over the course of six days starting at 2 weeks post assembly (wpa) and again at 8wpa. After acquisition, images were registered and aligned to generate a time series (Figure 10a). Comparing individual fasciculated axon tracts ("tract") across 2wpa and 8wpa image sets shows a progressive increase in tract complexity and density (Figure 10b). At the same time, tract polarity and directionality are preserved over these prolonged periods of time (Figure 10c), suggesting that our approach allows for stable and long-term assessment of axon pathfinding, targeting and tract formation.

To assess the implications of CNTNAP2 and ISLR2 on interhemispheric axon tract formation, we generated three different hiPSC lines, stably expressing the respective shRNA as well as an inducible GFP (Figure 11a,b). We then generated COAs by fusing mutant or control (shCNTNAP2, shISLR2, shNTC) to isogenic wild type FBOs (Figure 11c). Axon projections and tract formation were assessed at 2wpa and 8wpa. Notably, axon tracts were largely absent in COAs deficient for CNTNAP2– this was significantly different compared to the control condition (CNTNAP2 vs NTC, $P = 0.0238$, Mann-Whitney U Test, Figure 12f). The open source software Ilastik[24] was used to detect all GFP+ projections in the target side in an unbiased and unsupervised manner. At 2wpa, CNTNAP2-deficient COAs had significantly

less GFP+ projections extending into the wild type cortical unit as compared with control COAs (CNTNAP2 vs NTC, 4.74% vs 34.81%, *P* = 0.0286, Mann-Whitney U Test, Figure 12d)**.** There were no significant differences in overall GFP+ projections reaching the target cortical unit at 8wpa. Interestingly, while CNTNAP2-deficinency resulted in delayed innervation of the target region (Figure 13d), axon organization and fasciculation remained absent at all time points (Figure 12e and 13e). In contrast, ISLR2-deficiency did not severely alter early axon tract formation (2wpa; Figure 12e), but resulted in progressive dispersion at the expense of long-term tract maintenance (ISLR2 vs NTC, Mean 39.20% vs 8.36%, P = 0.0317, Mann-Whitney U Test, Figure 13f).These findings indicate that CNTNAP2 plays important roles during axon tract formation whereas ISLR2 appears to be more involved in processes that sustain tract integrity.

In summary, the experiments show that that our novel assembloid system allows to model processes relevant for human cortical development that can inform future studies to identify specific developmental implications for autism-associated risk genes.

DISCUSSION

Evidence from diverse postmortem and non-invasive imaging studies suggests that atypical brain connectivity in autism affects short and long-range cortical pathways[14,25,26].

We have established a system for modeling reciprocal axon connectivity between human cortical units in 3D cultures by targeted assembly of regionally-specified brain organoids. As demonstrated here, reciprocal neuronal connections are formed between COA hemispheres. We found these axons fibers to fasciculate and participate in organized pathfinding into the target hemisphere, where they established structural correlates of synapses. We further demonstrated successful long-range connectivity between COA hemispheres, using rabies tracing techniques. Finally, we showed that loss of CNTNAP2 or ISLR2 impacts axon outgrowth and fasciculation dynamics in the system. We observed that loss of CNTNAP2 impairs early axon tract formation and leads to less organized pathfinding routes, while loss of ISLR2 affects tract density at later stages and leads to early axonal dispersion. These results are in line with the proposed involvement of these genes in axon guidance and provide new insight into their direct and specific influence during human cortical development.

While existing studies provide important insight on the functional role of CNTANP2, several conflicting reports exist. This is predominantly due heterogenous approaches to modeling cortical development, and experimenter emphasis on different developmental time points. Our work compliments existing findings by identifying a population of DLPNs impacted by knock down of CNTNAP2 and ISLR2 expression. These findings clarify the relevance of both genes in ASD pathology and specificity to cortical networks. Work by

Peñagarikano et al. 2011 demonstrated migratory abnormalities, induced by CNTNAP2 knock out in mouse cortical neurons[13]. We did not detect and migratory abnormalities, when evaluating the impact of CNTNAP2 knock down. It is possible further effects of CNTNAP2 could be elucidated with a full knock out, as opposed to the partial knock down we used in our system. However, it is also unclear how the developmental timeline of stem cell generated models connects to that of in vivo mouse models. Considering the significantly slower development of the human cortex as compared to mice, long term culture of the COA system could reveal similar results as detected in mice aged 2-4 months. Additionally, work by Varea et al. 2015 did not detect any abnormalities in axon or dendrite outgrowth, when CNTNAP2 was knocked out in primary culture rat neurons at 3DIV[27]. Again, significant value should be placed on the timing of this study, as axon fasciculation happens after DLPNs finish migrating into the cortical plate, during late stage early development.

Further characterization of this model is also needed. Due to the complexity of the human brain, it is apparent that our forebrain-patterned organoid and assembloid models do not fully recapitulate the important developmental influences of brain regions or signaling pathways outside of the cortex. One such region is the thalamus, where ISLR2 regulates pathfinding between cortico-thalamic and thalamo-cortical projections and interbrain region integration[17]. However, recent advances have been made towards achieving assembloid models that can recapitulate cortico-thalamic pathways, but further research is needed to establish more complex systems. While mouse models are undoubtedly needed to study regional interactions during brain development from a holistic point of view, human-specific features may not be modeled. The Generating COAs from known patient cohorts that have been genetically profiled could reveal previously unknown trends in cortical development and new risk genes and pathologies; however, in vitro technology has several hurdles to overcome, notably: batch effect and reproducibility. One current problem specific to organoid

culture is the development of necrosis, at the organoid's core. This problem has been addressed by several groups and is in part ameliorated by shaking during culture, to increase media oxygenation[28]. Our slice culture system solves this problem, by dramatically increasing available surface area for media exchange. This allows for long term culture of organoid species, while preventing the confounding effect of tissue necrosis. Further improvements in the organoid differentiation paradigm could make this model cheaper and more efficient, allowing for experimenters to deploy it as a diagnostic approach to developmental disease.

It is likely that this model could be expanded to generate other inter-regional networks, notably the cortico-thalamic and thalamo-cortical circuitry identified as relevant to ASD, ADHD, and schizophrenia pathologies[29,30]. New developments in organoid technology may also allow for complex circuit reconstruction, such as the cortico-striatal-thalamic loop which has been identified as relevant in developmental disorders like ASD. This could significantly improve the diagnostic relevance of COAs, by faithfully recreating whole, intact circuits. This also would allow for modeling diseases not limited to cortical integration.

Ultimately, the flexibility and scalability of brain organoid models as well as our COAs makes them a suitable model for studying human developmental diseases. While new advances are necessary to perfect the technology, its reliance on human genetics and highly organized nature serve to provide new insights on classic disease pathologies, especially in the context of development. Future experiments may leverage many organoids integrated into a single assembloid, to replicate complexity near or approximate to the intact brain. Considering the limitations on available human tissue, the confounding variable introduced by studying independent tissue samples, and lack of time course samples, our COA system has wide spread relevance to the field of developmental biology, in the context of uniquely human diseases.

MATERIALS AND METHODS

iPSC Culture

A complete list of medias and supplements is available in Table 1 and 2, respectfully. Tissue culture incubators were kept at 37 °C, 5% CO2 and 20% O2. hiPSCs were cultured using commercial IPS Brew (Miltenyi Biotec) in 6 well plates coated with 80 µg/well of Matrigel (Cultrex #3433-005-01). Cells were fed daily with 2mL of media per well. Cells were allowed to reach 70% confluence, before passaging. Passaging was done with Gentle Cell Dissociation Reagent, from Stem Cell Technologies (Stemcell technologies #07174). Cells were diluted to achieve 30% confluence after passaging. Cells were discarded after reaching 55 passages, to avoid karyotypic abnormalities.

For virus production, 293t cells were cultured in DMEM+ GlutaMAX supplemented with 5% heat-inactivated FBS. Cells were passaged using TripLE reagent (Gibco #12604013), after reaching 90% confluence. If needed, cells were passed through a 40µm cell strainer to remove clumps and achieve even plating distribution (VWR #10199-655).

Virus Generation

Lentiviruses and retroviruses were generated using 293t cells, cultured in DMEM GlutaMAX supplemented with 5% heat-inactivated FBS. 7x10^6 cells were plated on 15cm dishes (Falcon #353025), the day before transfections. For transfection, the following were combined in a 50mL tube: 12.2µg vector plasmid, 8.1µg PMDL plasmid, 3.1µg REV plasmid, 4.1µg pMD2.G plasmid, 110µL PEI and 1mL Optimem, per plate of cells. Media was

changed exactly 5 hours after transfection. For lentiviruses: a single collection of media was made 3 days post transfection. For retroviruses: media was harvested 2 days post transfection and replaced with fresh media. The fresh media was harvested the next day. Virus was concentrated by spinning at 19,800 RPM for 2 hours at 4 °C. The resulting viral pellet was dislodged and resuspended in 5μL DPBS + Glucose per plate of cells collected. All virus was immediately stored at -80 °C

Retroviral birth dating and Neuron Tracing

Retroviruses were titered by serial dilution. 150k 293t cells were plated in a 6 well plate, the day before starting the titer test. 2μL of retrovirus was added to the first well and serial diluted 1:10 for each subsequent well. Titer was determined by the concentration at which 10% of cells were infected. Organoids were birth-dated with 5μL of pRV-CAG:GFP at 28 DIV. Organoids were harvested after 2 weeks and 6 weeks of infection. Specimens were fixed, sectioned and subsequently stained for GFP to enhance signal. Even numbered slides were stained for GFP, CTIP2, and MAP2 (Table 3). Slides were then imaged with the Zeiss Confocal LSM 880 system. Images were exported as tiff files and uploaded to the commercial tracing software Neurolucida[23]. Neurons were reconstructed and the absolute distance from each soma to the ventricular zone was measured. To quantify complexity, Sholl analysis with starting radius 5μm and increments of 5μm was performed on the traced neurons. Only cells double-labeled for DLPN marker CTIP2 and GFP were selected for tracing and soma tracking.

Generation of Stable iPSC

H1 and H9 Embryonic Stem Cells as well as a normotypical hiPSC line were used in this study. H1 ESCs were used for WT experiments without endogenous GFP expression. H9 ESCs were used to generate a stable expressing line from pLV-CAG:eGFP. hiPSCs were used to generate three lines: pLV-TRE-eGFP-U6-shNTC, pLV-TRE-eGFP-U6-shCNTNAP2, and pLV-TRE-eGFP-U6-shISLR2. To generate stable lines, three wells of a six well plate were grown to low confluency (30% confluent). Two wells were treated with 5μL of concentrated lentivirus for 24 hours. The third well served as control well for puromycin administration. Media was replaced with standard IPS brew 24 hours later. Cell lines were then grown until highly confluent (70% confluent), to ensure plasmid expression. Cells were then passaged to 30% confluence. After passaging, culture media was supplemented with 1μg/mL puromycin. 24 hours later, media was replaced with a lower concentration puromycin (0.5μg/mL). Puromycin media was replaced every day, for three days. Cells were fed and maintained according to normal procedure, following selection. GFP expression was induced by administering doxycycline at 5μg/mL, starting on Day 14 and onward.

FBO Protocol and Fusion Protocol

FBOs were generated based on a published protocol by Schafer et al. 2019[9]. FBOs were generated from 70% confluent hiPSC cultures. On Day 0, cultures were dislodged by incubating with 1mL Collagenase IV (1.5mg/mL). After detaching, intact colonies were gently washed with DMEM F12 to remove excess enzyme, and then transferred to a 10cm ULA dish (Corning #3262). At this stage, colonies were suspended in DMEM F12 Media supplemented with 10nM ROCK-inhibitor and 20ng/mL FGF2 to prevent cell death and promote the formation of EB aggregates. The next day, aggregates were washed and

transferred to Patterning Media supplemented with 2μM A83 and 2μM Dorsomorphin. Media was changed every other day. On Day 5, patterning media was replaced with Neural Induction Media (NIM), supplemented with 4ng/mL Wnt3A, 1mM CHIR, and 1mM SB. On day 7, EBs were selected for embedding in 20μL of Matrigel (Cultrex #3433-005-01). On Day 14, NIM was replaced with Differentiation Media (Diff), supplemented with 2.5μg/mL insulin – at this stage, dishes were transferred to an orbital shaker set to 90rpm. On Day 20, Matrigel was manually removed using a scalpel and p200 pipette. On Day 70, media was changed to Mature Forebrain Organoid Differentiation Media (MFBOM) for continued culture.

Assembloid Protocol

Assembloids were generated by fusing two FBOs at 28 days in vitro (DIV). Fusion took place in a 5mL polypropylene falcon tube (Corning #352063), filled with 2mL of media. Media was changed every 2 days, to avoid separating the forming assembloid. Assembloids were transferred back to standard culture conditions after five days**.**

Cryosectioning and Immunofluorescence

Organoids and assembloids were fixed using 4% PFA solution at pH 7.4, on ice. Prior to fixation, tissues were washed in TBS on ice, to elute any remaining media and to remove debris. Fixation was over a period of 40 minutes with constant, slow agitation on a shaker. Samples were washed after fixation to remove excess PFA, and immediately transferred to 30% with 0.5% NaAzide for cyro-protecting. For cryostat sectioning and long-term storage at -80 °C, samples were mounted in Tissue Freezing Media (General Data Company #TFM-Clear). Once frozen, organoids were sectioned at 50μm thickness, using a Leica Cryostat.

Sections were rinsed in TBS and then blocked for one hour in TBS++ containing 0.25% Triton-X100 (Thermo #28313) and 3% Normal Serum. Primary antibodies were incubated overnight at 4 °C, in blocking solution. The next day, slides were rinsed in TBS and incubated in blocking solution for 15 minutes. Secondary antibodies were added to the same solution at 1:500 concentration for two hours. Finally, sections were stained with DAPI 1:4000 in TBS and rinsed before cover slipping with Immu-Mount (Fisher #9990402).

Electrophysiology Protocol

Field potentials were generated and recorded using a dual electrode system. The stimulating electrode consisted of a single, grounded platinum electrode delivering a single, symmetrical 5V pulse with duration 10ms. The recording electrode consisted of a 12-15 mega ohm borosilicate capillary (Sutter #BF150-75-10), filled with intracellular solution. The sample was immersed in standard formulation artificial cerebral spinal fluid and maintained at 34 °C. Field potentials were recorded both in the target GFP- organoid and separately recorded in the source GFP+ organoid. The stimulation electrode was placed in the source GFP+ organoid, as far from the assembloid fusion site as possible.

EM Protocol

Tissue fixation, array tomography immuno-fluorescence, and EM imaging were performed according to Micheva and Phend, 2017[31]. Prior to this procedure, all reagents were baked to total dehydration. Tissue was first fixed in a 2% Glutaraldehyde / 2% paraformaldehyde in phosphate buffer. Following fixation, the sample was dehydrated using the freeze-substitution method, for high quality preservation of cellular membranes. Initial

cryoprotection in 10%, 20% and finally 30% over night was used for additional protection of membranes. The AFS unit was set for -90°C for 32 hours, and then raised +4 °C/h until reaching -45°C. Sample was held at -45°C for 50h, then temperature was raised by +5°C/h until reaching 0°C. Sample was held at 0°C for 40h. Samples were embedded in Lowicryl HM-20 (Electron Microscopy Sciences #14340)and subject to UV curing. To ensure even curing, samples were flipped after 24 hours. Resulting blocks were sectioned at 70nm thickness using an ultramicrotome and deposited onto silicon wafers. Sections were etched using 1% NaBH4 (Sigma #S9125) in TBS. Following etching, samples were incubated with 50mM glycine to block autofluorescence. Sections were blocked with 0.05% Tween-20 (Electron Microscopy Sciences #25564) and 10% BSA-C (Aurion BSA-C), to further reduce background signal. GFP Chicken antibody was used at 1:50 concentration in blocking solution, and incubated at 4°C overnight. Following primary incubation, sections were rinsed with filtered TBS and secondary antibody was added at 1:500 concentration in blocking buffer. After two hours, secondary antibody was removed and sections were rinsed in TBS.

Generation and Characterization of shRNA

shRNA constructs were chosen based on the Broad Institute RNAi algorithm[32] (Table 4). shRNA constructs were cloned into lentiviral and retroviral vectors. Full vector maps are available in supplemental methods. Plasmids were sent for Sanger sequencing, to verify plasmid integrity. Neural progenitor cells (NPCs) were electroporated with the plasmids, to determine knock down efficiency. Electroporation was done with high confluency NPCs, using the Amaxa Nucleofector 2b electroporation system (Lonza #VPG-1005). Each reaction was performed with 3 million cells and 1µg plasmid. Each reaction was plated separately, in a 24 well plate. 24 well plates were necessary to minimize spontaneous differentiation of

NPCs. Plates were coated with 10µg/mL Poly-L-Ornithine and 5µg/mL Laminin, to promote cell adherence. Following electroporation, NPCs were treated with 1µg/mL puromycin for 24 hours and then harvested using Trizol (ambion #15596018) reagent.

RNA Extraction and qPCR Validation of Expression

RNA was extracted from cells and whole organoids dissociated in Trizol reagent (ambion #15596018). RNA extraction was performed using the phase separation method, and stained for visibility with GlycoBlue (Invitrogen #AM9515). Following extraction, samples were tested for concentration and purity using the Invitrogen Qubit system and reverse transcribed with the Invitrogen Super Script III kit with oligo DT primers (Invitrogen #18080051). The qPCR reactions were performed with 70ng of DNA, 0.5 µM forward and reverse primer (Table 5), and SybrGreen Master Mix from ABI (ABI #4364344). Samples were run in triplicate, to identify possible outliers. A product melt curve was also measured, to ensure sample quality.

Slice Culture and Vibratome

Organoids and assembloids were sectioned using a Leica VT1000 S vibratome. Samples were sectioned at 500µm, with the vibratome set to 90 Hz frequency and 0.01mm/s speed. Immediately after sectioning, slices were incubated in media supplemented with 1x anti-anti. After sectioning, samples were transferred to a Corning collagen coated cell culture insert (Costar ref# 3450). Inserts were equilibrated with culture media before use. Inserts were filled with 500µL of media above the insert and 2mL of media below the insert. Slices were allowed to recover over 5 days before performing further experiments.

Live Imaging and Image Analysis

Live slices were imaged on a Zeiss CSU Spinning Disk Confocal Microscope, every 48 hours. For imaging, intact tissue culture Inserts were transferred to a 5 cm glass bottom dish, with 500µL of media. The dish lid was parafilmed and punctured, to prevent dehydration during overnight imaging but still allow gas exchange. A long working distance objective was used (Zeiss EC-PLAN-NEOFLUAR 20x LWKD), to ensure the sample was within the focal range of the objective. Samples were imaged at standard tissue culture conditions. After acquisition, images were exported as maximum intensity projections, using the commercial software, Zen Blue[33]. After export, images were binarized using the open source software, Ilastik[24]. Following binarization, FIJI[34] was used to segment images, quantify the relevant ROIs, and export area percentages.

FIGURES

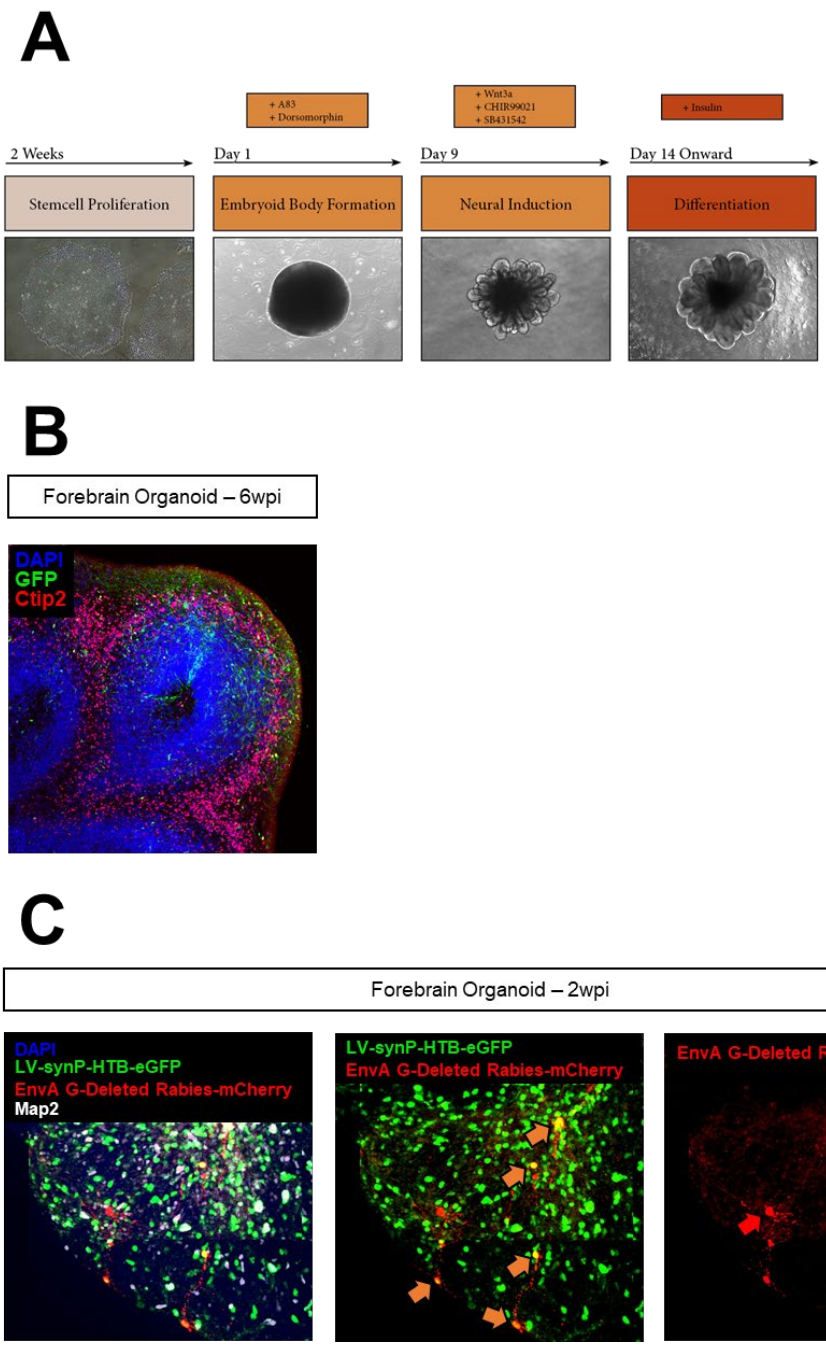

Figure 1: FBOs display complex morphology and local connectivity

A, Schematic of dual SMAD inhibition and forebrain patterning of organoid species
B, Retroviral birth-dating demonstrating selective labeling of CTIP2+ neurons. Administered at 28DIV. By 6wpi, neurons migrate into cortical plate and develop arborization.
C, G-Deleted rabies demonstrating local connectivity in FBO. Orange arrow indicates GFP+/mCherry+ neuron. Red arrow indicates mCherry+ neuron

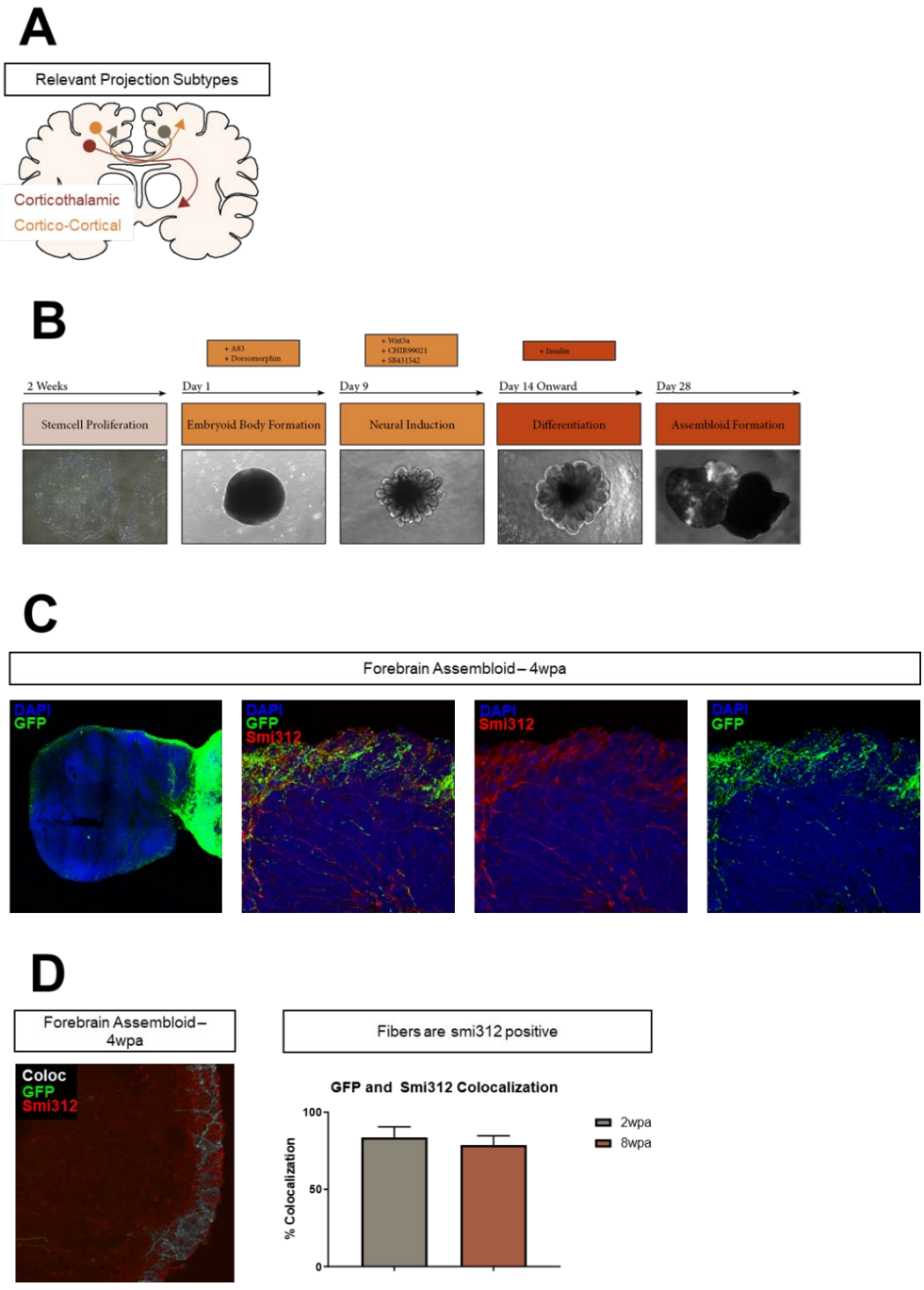

Figure 2: COAs demonstrate reciprocal inter-cortical connectivity

A, Schematic of long-range projection subtypes
B, Modeling inter-cortical connectivity with COAs derived from FBOs
C, COA units demonstrating a high level of interconnectivity, with GFP+ projections in target organoid cortical regions
D, GFP+ Projections strongly colocalize with smi312, indicating axonal identity

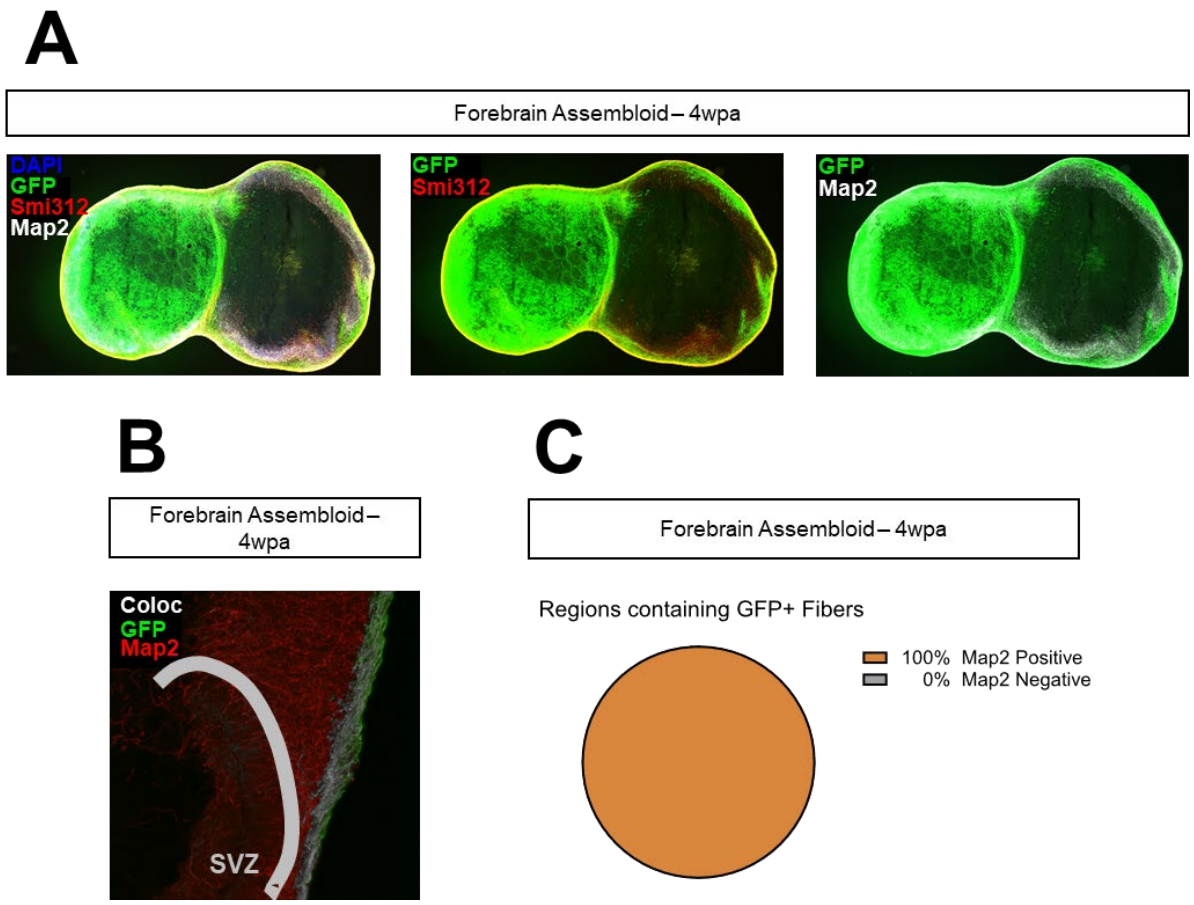

Figure 3: COAs establish axonal projections onto neuronal targets in an organized fashion

A, GFP+ axons project into superficial, cortical regions of target organoid
B, GFP+ axons highly colocalize with MAP2+ regions in target organoid
C, GFP+ axons project in an organized fashion, by exclusively innervating MAP2+, neuronal regions in target organoid

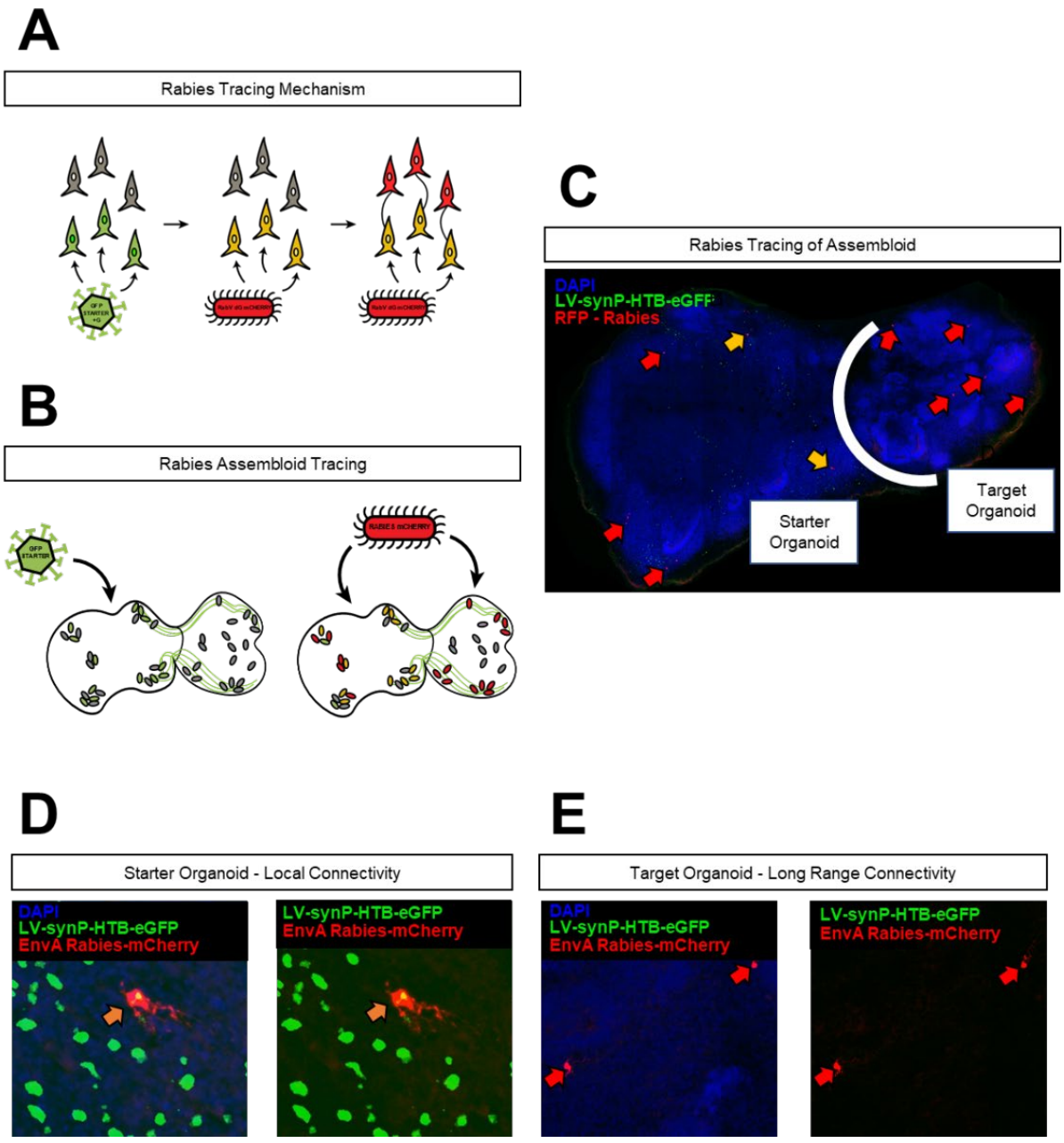

Figure 4: COAs recapitulate local and long-range connectivity

A, Schematic of G-Deleted rabies virus system demonstrating population specific, retrograde, monosynaptic tracing. Schematic adapted from Kim et al. 2016 [21]
B, Schematic demonstrating application of hSyn::HTB-GFP helper virus to establish starter population, and administration of RV-dG CAG::mCherry making monosynaptic jump across fusion plate
C, Overview of rabies-traced connectivity in COA. Orange arrows indicate double positive GFP+/mCherry+. Red arrows indicate mCherry+. Starter cells are located exclusively in the starter organoid.
D, Example double labeled GFP+/mCherry+ cell demonstrating local connectivity
E, Example single labeled mCherry+ cells demonstrating long range connectivity – note absence of GFP+ starter cells

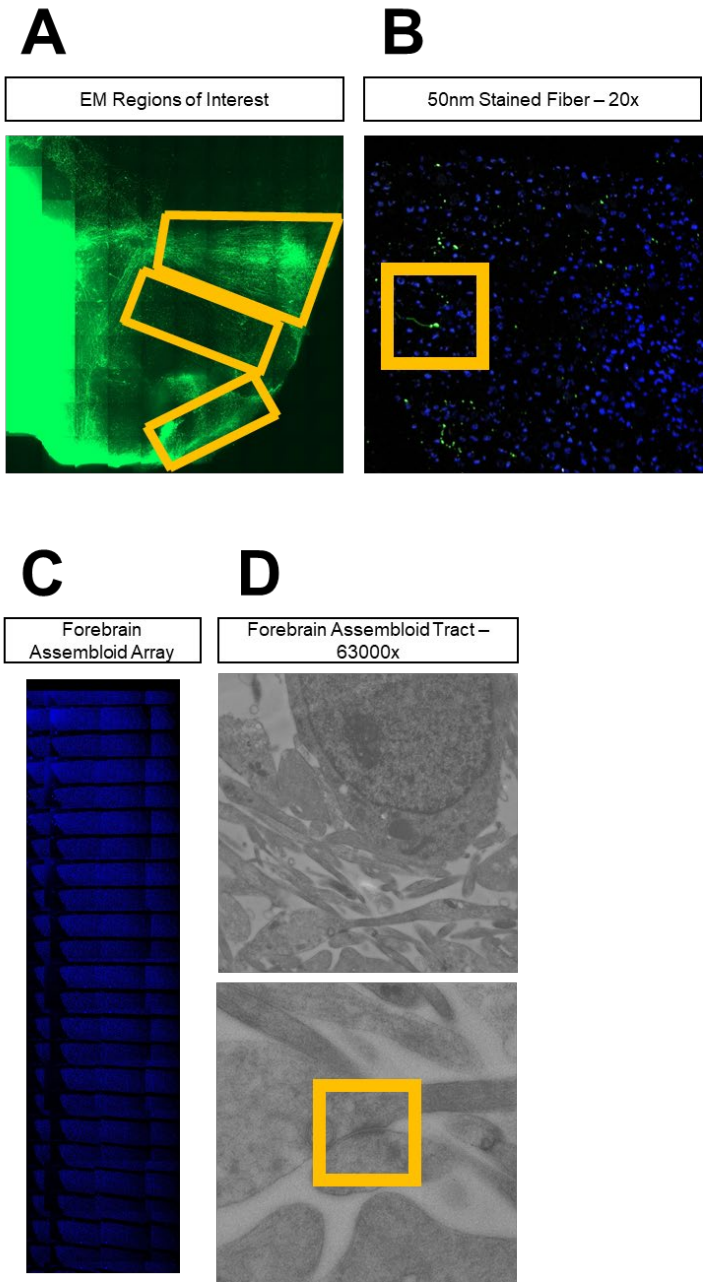

Figure 5: Electron microscopy and correlative array tomography immuno-fluorescence yielded a putative synapse

A, Micro-dissection of three regions of interest, in proximity to GFP+ axon fibers present in the target organoid
B, Example GFP+ axon fiber from starter organoid detected by IF for GFP
C, Overview of stained array to be correlated with SEM-imaging
D, 63000x magnification SEM Image showing putative synapse. Bottom panel digitally zoomed.

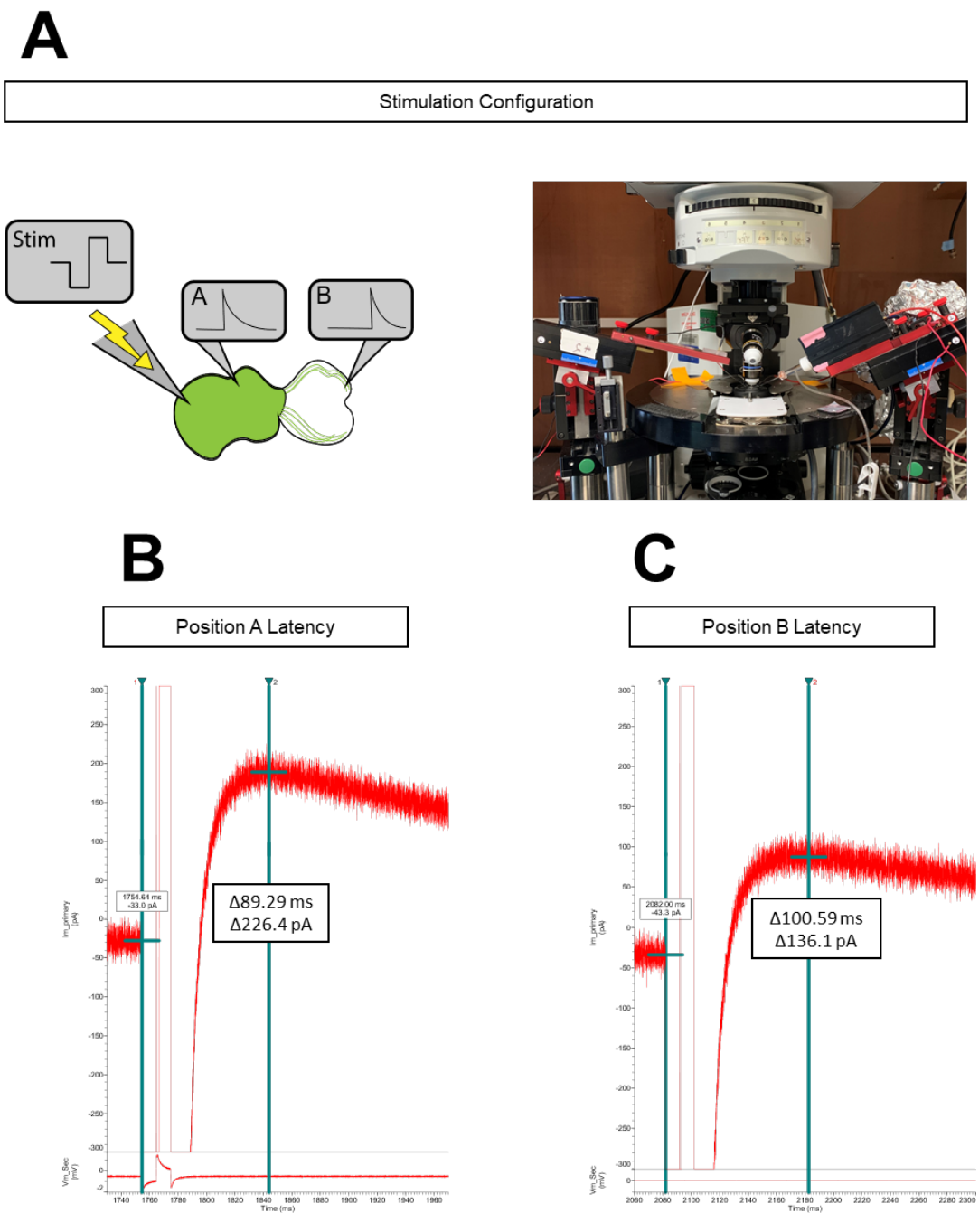

Figure 6: Evoking local and long-range potentials in COAs

A, Schematic and image of stimulation and recording setup, showing the two different recording electrode positions and placement of the stimulating electrode
B, Trace of locally evoked field currents, by stimulating and recording from GFP+ “hemisphere”
C, Trace of long-range evoked field currents with lower amplitude and higher latency, after moving electrode to a distal region of the target organoid

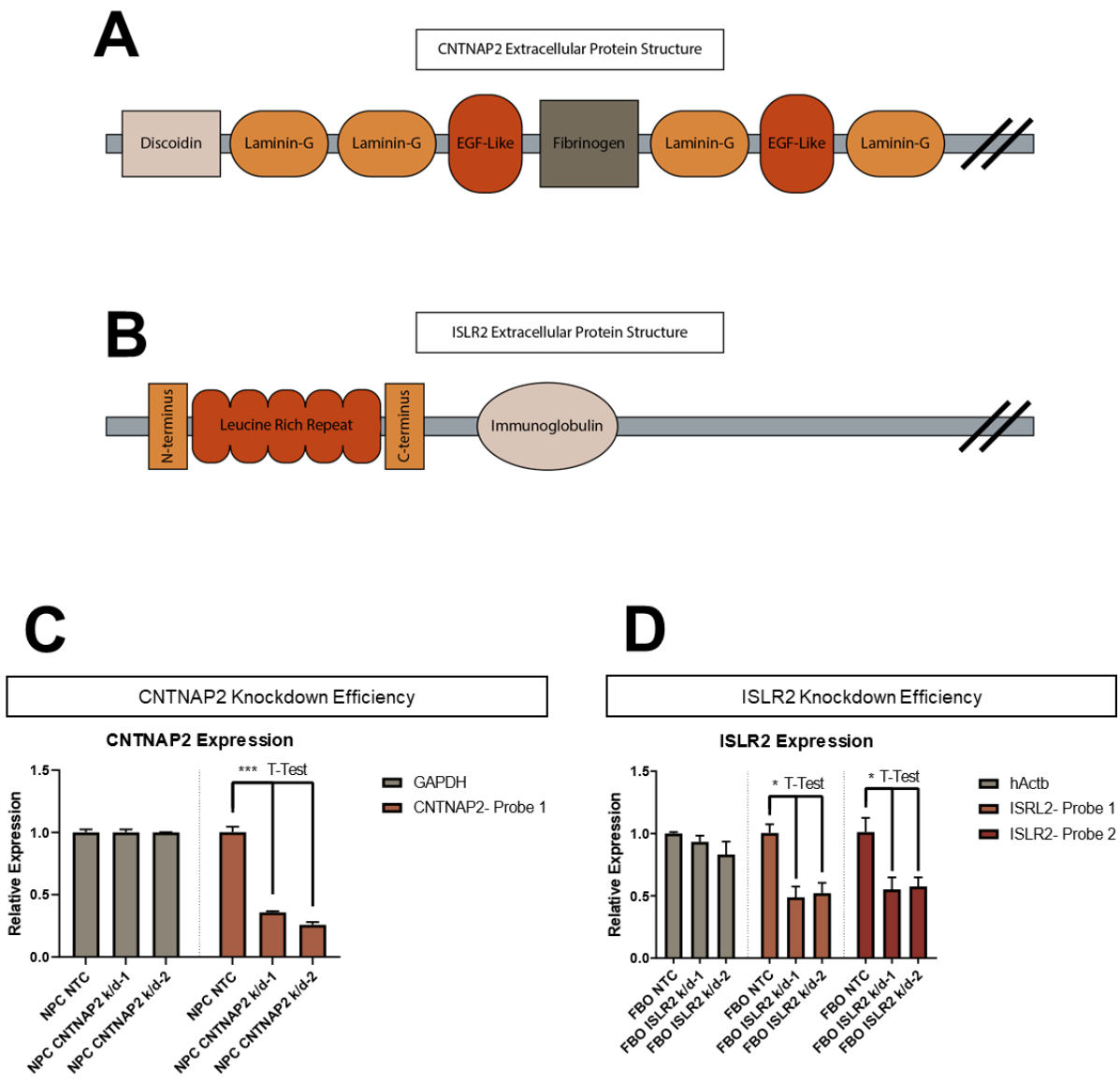

Figure 7: Targeting and efficiency of shRNA constructs

A, Schematic of Caspr2 protein encoded by CNTNAP2 with functional domains annotated. This figure was adapted from Poot 2015 [10]
B, Schematic of protein encoded by ISLR2 with functional domains annotated. This figure was adapted from Panza et al. 2015[15]
C, Evaluation of knock down efficiency of CNTANP2 in human NPCs. CNTANP2 expression is reduced to near 30% of control NTC expression level
D, Evaluation of knock down efficiency of ISLR2 in the shISLR2 hiPSC line. ISLR2 expression is reduced to near 50% of control NTC expression level

Figure 8: Evaluating cortical migration and morphology with retroviral birth dating

A, Retroviral construct used for birth dating neurons with GFP and expression of targeted shRNAs
B, Example stains of CTIP2+ and GFP+ neurons migrating into the CP for each condition
C, Example reconstruction of CTIP2+ and GFP+ neurons for each condition
D, Complexity and morphology of CTIP2+ neurons are not impacted by CNTNAP2 or ISLR2 kd
E, ISLR2 kd impacts migration of CTIP2+ neurons, by significantly reducing migratory distance traveled

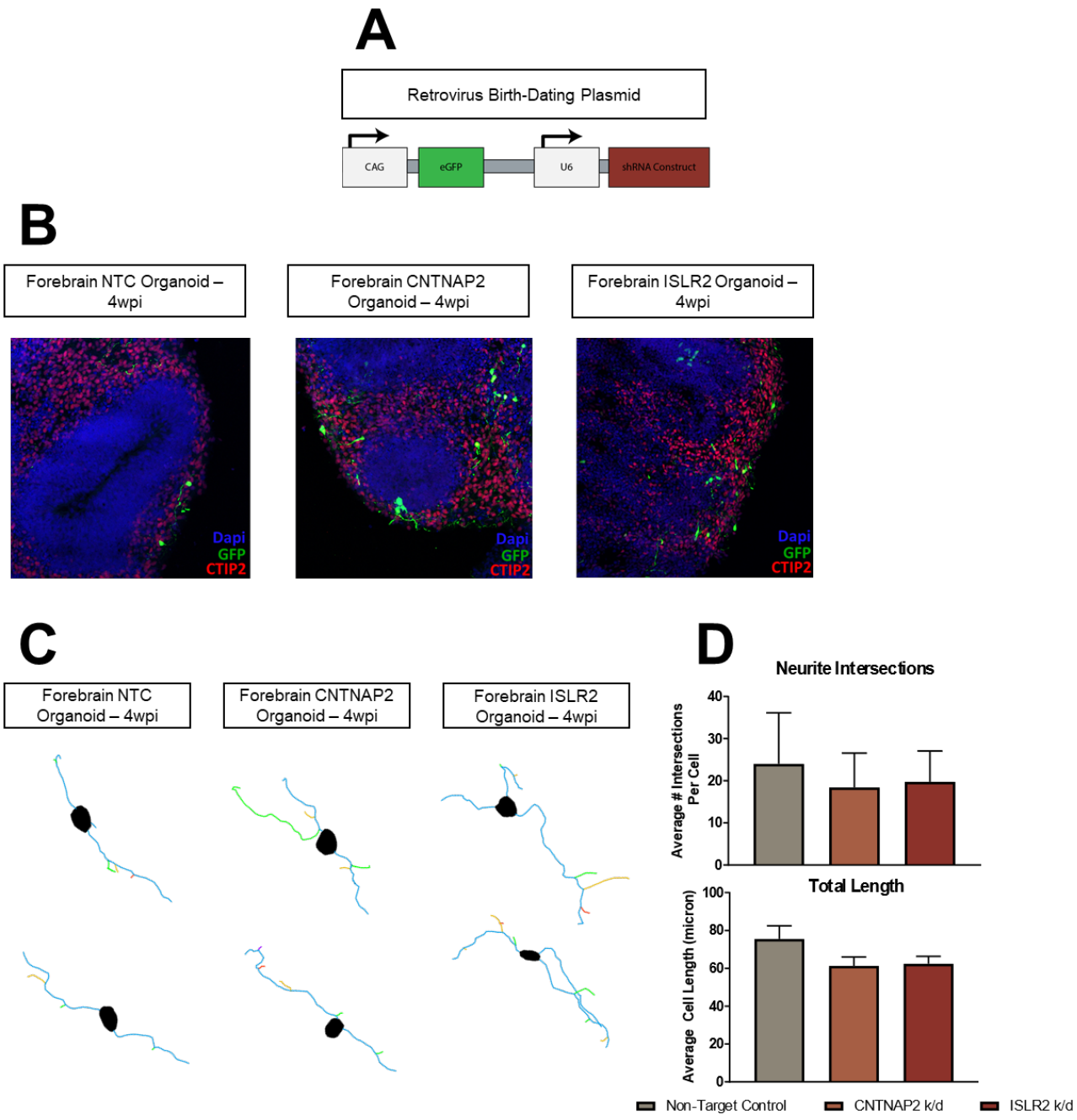
A
Retrovirus Birth-Dating Plasmid
CAG
eGFP
U6
shRNA Construct
B
Forebrain NTC Organoid – 4wpi
Forebrain CNTNAP2 Organoid – 4wpi
Forebrain ISLR2 Organoid – 4wpi
Dapi
GFP
CTIP2
C
Forebrain NTC Organoid – 4wpi
Forebrain CNTNAP2 Organoid – 4wpi
Forebrain ISLR2 Organoid – 4wpi
D
Neurite Intersections
Average # Intersections Per Cell
Total Length
Average Cell Length (micron)
Non-Target Control
CNTNAP2 k/d
ISLR2 k/d
E
Migratory Distance
**** MW U-Test
Migratory Distance (microns)
Non-Target Control
CNTNAP2 k/d
ISLR2 k/d

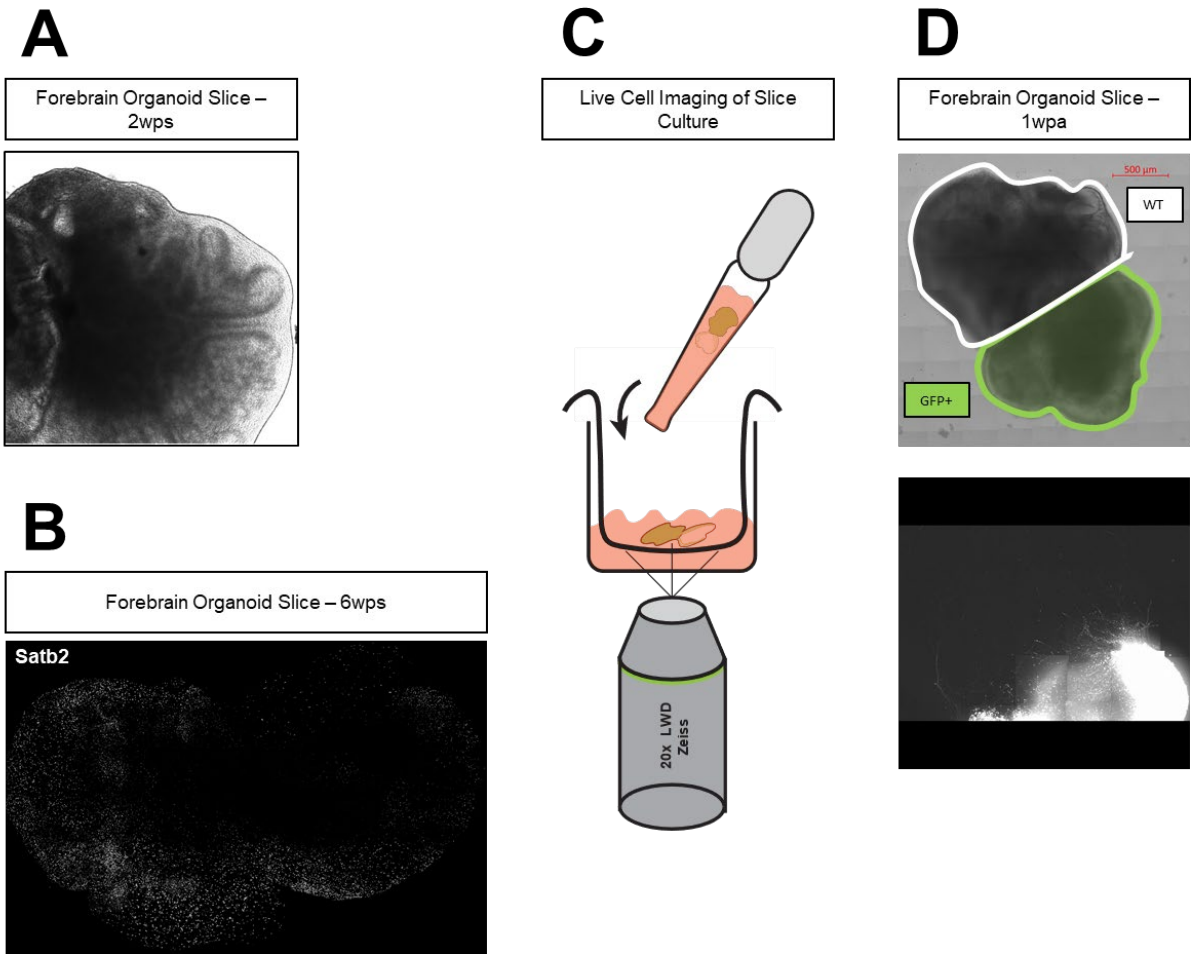

Figure 9: COA slice culture system enabling longitudinal, live cell imaging

A, Brightfield image of COA slice, showing intact VZ and CP regions after slicing
B, SATB2+ population present 6wps, due to improved media exchange in slice culture system
C, Schematic of live cell imaging setup using tissue culture inserts in a glass bottom dish
D, Overlay denoting GFP+ source FBO and GFP- WT FBO, in COA. Bottom panel illustrates live cell imaging of GFP signal

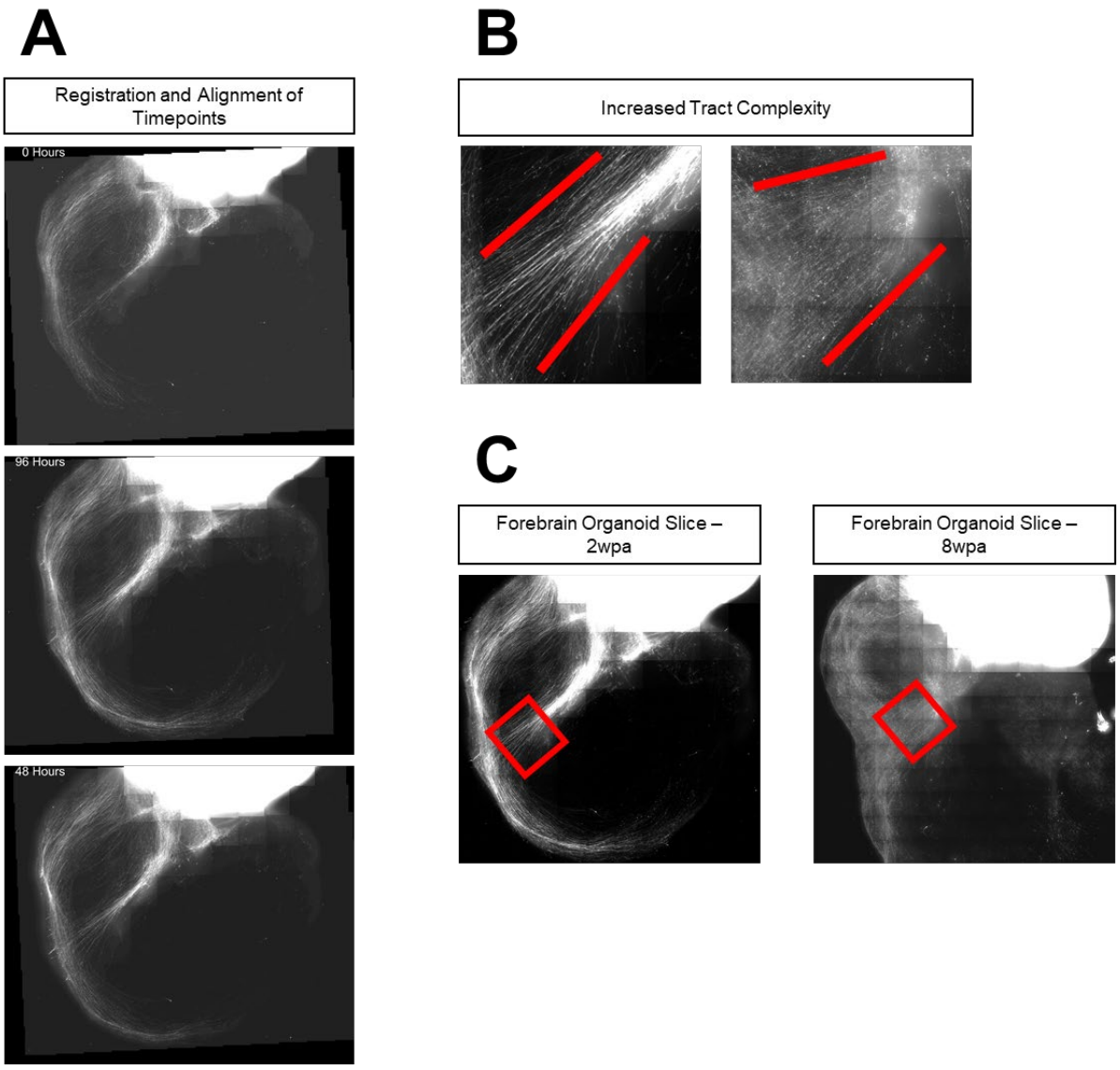

Figure 10: Axon fascicules increase in complexity while preserving polarity and organization

A, Registration and alignment of slice culture images after acquisition, demonstrating tract elongation and thickening
B, Axon tracts increase in density and complexity, between 2wpa (left) and 8wpa (right)
C, Axon tracts maintain overall morphology and polarity, between 2wpa and 8wpa

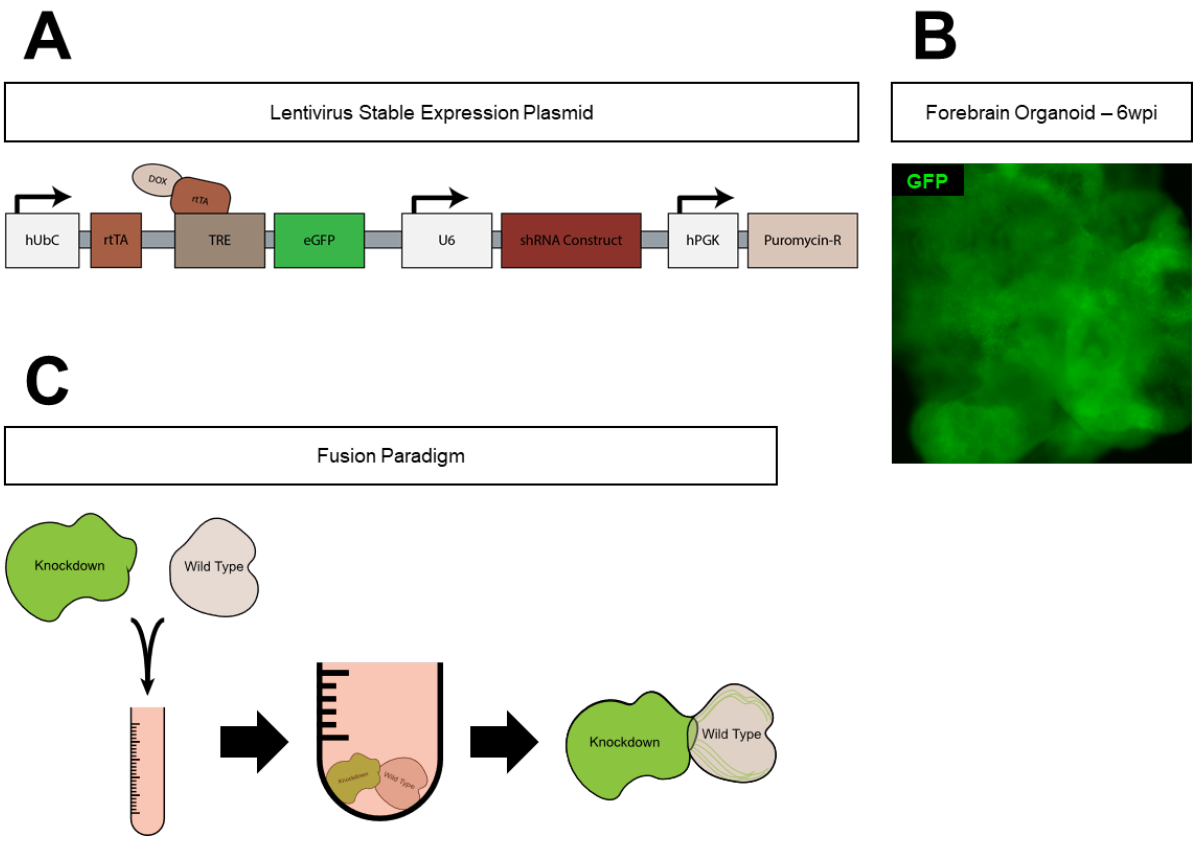

Figure 11: Generation of knock down, GFP+/GFP- assembloids

A, Schematic of the lentiviral construct used for stable line generation to express shRNAs and inducible GFP
B, Induced, global expression of GFP in FBO generated from pLV-TRE-eGFP-U6-shNTC, after selecting hiPSCs with puromycin
C, Schematic of knock down GFP+/GFP- assembloid formation in a falcon tube at 28DIV

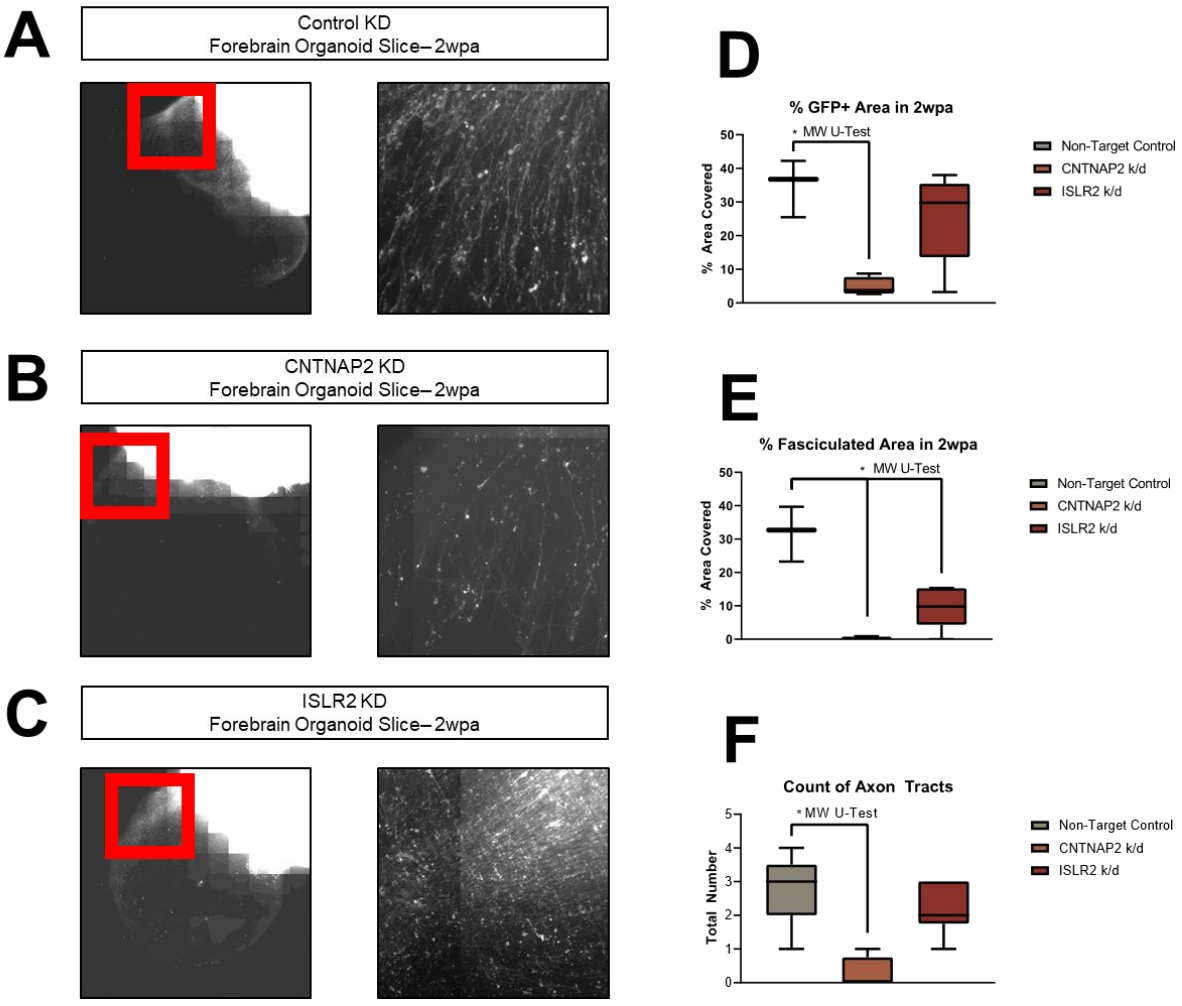

Figure 12: Knock down of CNTNAP2 and ISLR2 impact interhemispheric axon tract formation at 2wpa

A, Normal axon tract formation in COA expressing NTC kd, digital zoom (right)
B, Absent axon tract formation in COA expressing CNTNAP2 kd, digital zoom (right)
C, Decreased axon tract formation in COA expressing ISLR2 kd, digital zoom (right)
D, Comparison of axon outgrowth area at 2wpa. Axon outgrowth is significantly decreased in the CNTNAP2 kd, compared to the control condition
E, Comparison of fasciculated area present at 2wpa. Both the CNTNAP2 kd and ISLR2 kd have significantly less fasciculated area, compared to the control condition
F, Binary count of axon tracts present in each condition. Axon tracts are absent in the CNTNAP2 kd sample

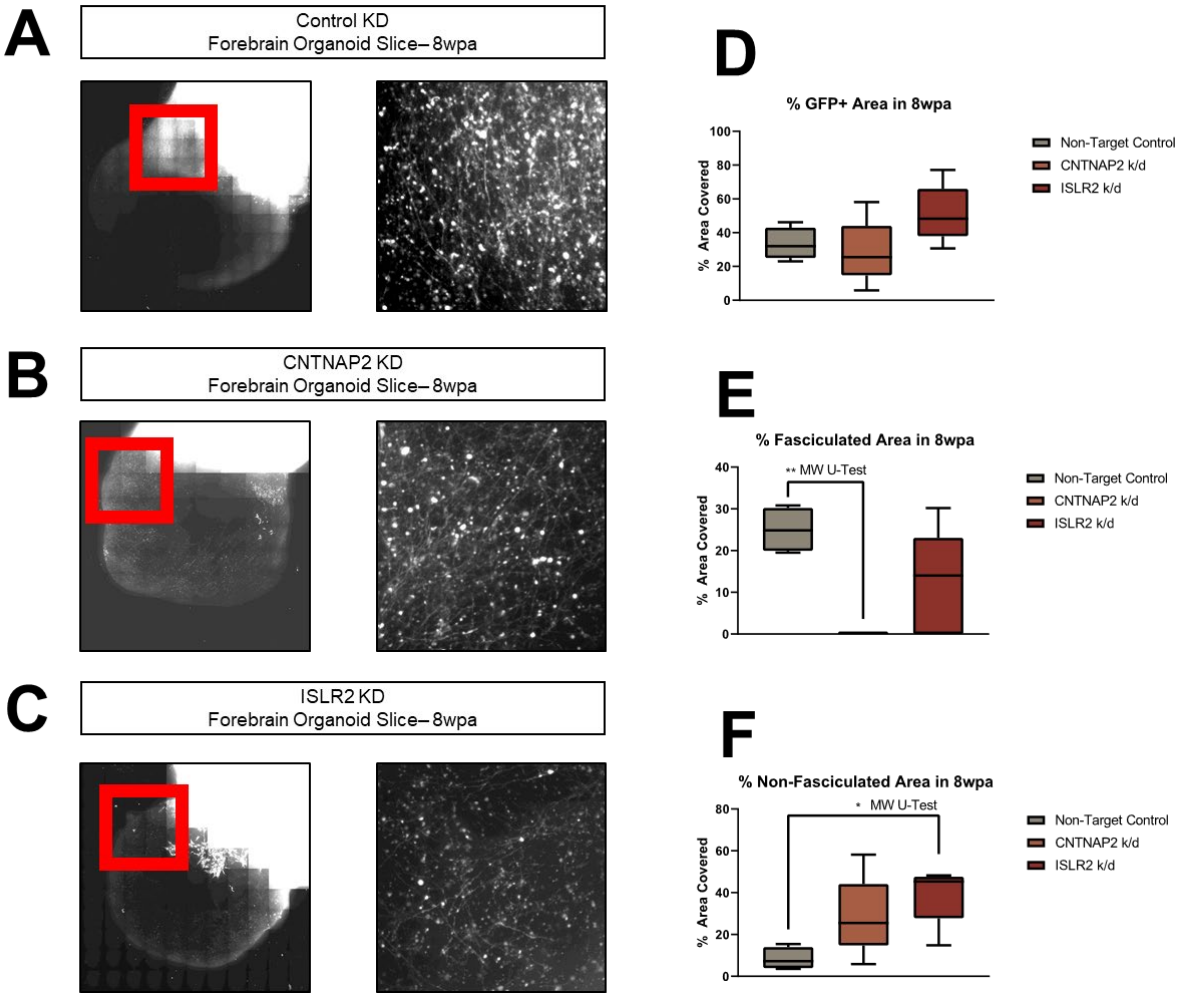

Figure 13: Knock down of CNTNAP2 and ISLR2 impact interhemispheric axon tract formation at 8wpa

A, Normal axon tract formation in COA expressing NTC kd, digital zoom (right)
B, Diffuse axon tract formation in COA expressing CNTNAP2 kd, digital zoom (right)
C, Diffuse axon tract formation in COA expressing ISLR2 kd, digital zoom (right)
D, Comparison of axon outgrowth area at 8wpa with no significant difference detected
E, Comparison of fasciculated area present at 8wpa, with significant disparity between control and CNTNAP2 kd
F, Comparison of non-fasciculated area present at 8wpa, with significant increase in aberrant outgrowth detected in the ISLR2 kd sample.

TABLES

Table 1: FBO and COA culture media formulation

Day 0 Media	
DMEM F12+ Glutamax	
1x	NEAA
55nM	2-Mercaptoethanol
20% (v/v)	KOSR
20ng/mL	FGF2
10nM	ROCKi
Patterning Media	
DMEM F12+ GlutaMAX	
1x	NEAA
55nM	2-Mercaptoethanol
20% (v/v)	KOSR
2µM	A83
2µM	Dorsomorphin
Neural Induction Media	
DMEM F12+ GlutaMAX	
1x	N2
1x	Pen / Strep
1x	NEAA
10µg/mL	Heparin
4ng/mL	Wnt 3A
1mM	CHIR99021
1mM	SB431542
Diff Media	
DMEM F12+ GlutaMAX	
1x	N2
1x	B27
1x	Pen Strep
1x	NEAA
55nM	2-Mercaptoethanol
2.5µg/mL	Insulin
MFBO Media	
Neurobasal Media	
1x	B27
1x Pen Strep	Pen Strep
1x GlutaMAX	GlutaMAX
1x NEAA	NEAA
0.2mM Ascorbic Acid	Ascorbic Acid
20ng/mL	GDNF
20ng/mL	BDNF
0.5mM	cAMP

Table 2: Tissue culture supplements, base medias and vendors

Base Media	Vendor
DMEM F12	Gibco #11330-32
DMEM F12 GlutaMAX	Gibco #10565-018
DMEM GlutaMAX	Gibco #10566-016
ips Brew	Mylteni #130-104-368
Neurobasal-A	Gibco #10888-022

Supplements	Vendor
2-Mercaptoethanol	Gibco #21985023
A83	AdooQ #A12358-50
Accutase	StemCell Tech #AT-104
Anti-Anti	Gibco #15-240-062
Ascprbic Acid	StemCell Tech #72131
B27	Life Tech #17504044
BDNF	Peprotech #450-02
cAMP	TOCRIS #1141
CHIR99021	AdooQ #A10199-100
Collagenase IV	Gibco #17104-019
Dorsomorphin	Tocris #3093
Doxycycline	Stemcell Technologies #72742
DPBS + Glucose	Gibco #14287-072
FGF2	Join Protein Central
GDNF	Peprotech #450-10
Glutamax	Gibco #35050-061
Heparin	Sigma #H3149
Insulin	Sigma #I9278-5ml
KOSR	Gibco #10828028
Laminin	Invitrogen #A25607
MEM NEAA	Gibco #2028870
N2	Life Tech #17502048
Pen / Strep	Gibco #15140-122
Poly-L-Ornithine	Sigma #P3655
Puromycin	Gibco #A11138-03
ROCKi	StemCell Technologies #72308
SB431542	StemRD #SB-050
Wnt 3A	R&D #5036-WN

Table 3: Primary antibodies, vendors and applicable concentrations

Antibody	Vendor	Concentration
GFP	Life Tech #A-11122	1:1000
GFP	Abcam #ab5450	1:1000
GFP	Aves Labs #GFP-1020	1:2500
RFP	Abcam #AB205402	1:1000
Satb2	Abcam #92446	1:500
Ctip2	Abcam #ab18465	1:400
Map2	Abcam #ab5392	1:1000
Smi312	BioLegend #837904	1:2000

Table 4: shRNA oligo sequences

shRNA Sequences	
CNTNAP2 shRNA 1 FW	CCGGCCTAGAGAGATACCACGGTTACTCGAGTAACCGTGGTATCTCTCTAGGTTTTTG
CNTNAP2 shRNA 1 RV	AATTCAAAAACCTAGAGAGATACCACGGTTACTCGAGTAACCGTGGTATCTCTCTAGG
CNTNAP2 shRNA 2 FW	CCGGGATGAGCCAAATCGATATTTCCTCGAGGAAATATCGATTTGGCTCATCTTTTTG
CNTNAP2 shRNA 2 RV	AATTCAAAAAGATGAGCCAAATCGATATTTCCTCGAGGAAATATCGATTTGGCTCATC
ISLR2 shRNA 1 FW	CCGGTATTAGGGAGTGGGCCGATTTCTCGAGAAATCGGCCCACTCCCTAATATTTTTG
ISLR2 shRNA 1 RV	AATTCAAAAATATTAGGGAGTGGGCCGATTTCTCGAGAAATCGGCCCACTCCCTAATA
ISLR2 shRNA 2 FW	CCGGCGTTTCTAACCACGCGTTCAACTCGAGTTGAACGCGTGGTTAGAAACGTTTTTG
ISLR2 shRNA 2 RV	AATTCAAAAACGTTTCTAACCACGCGTTCAACTCGAGTTGAACGCGTGGTTAGAAACG

Table 5: qPCR probe sequences

qPCR Probes	
CNTNAP2 Probe F	TTACACTTGGTGGGTTGGCA
CNTNAP2 Probe R	AGCATCCTTCCTCCATTGCTT
ISLR2 Probe 1 F	GACCGTGTGTCTGCTTGAGA
ISLR2 Probe 1 R	CCGCTTTTACGCCCTGCTC
ISLR2 Probe 2 F	ACCGTGTGTCTGCTTGAGAG
ISLR2 Probe 2 R	CCGCTTTTACGCCCTGCTC

REFERENCES

1. CDC. Data and Statistics on Autism Spectrum Disorder | CDC. *Centers for Disease Control and Prevention* https://www.cdc.gov/ncbddd/autism/data.html (2020).

2. Courchesne, E. & Pierce, K. Why the frontal cortex in autism might be talking only to itself: local over-connectivity but long-distance disconnection. *Curr. Opin. Neurobiol.* **15**, 225–230 (2005).

3. About SFARI Gene. *SFARI Gene* https://gene.sfari.org/about-sfari-gene/.

4. Zweier, C., de Jong, E. K., Zweier, M., Orrico, A., Ousager, L. B., Collins, A. L., Bijlsma, E. K., Oortveld, M. A. W., Ekici, A. B., Reis, A., Schenck, A. & Rauch, A. CNTNAP2 and NRXN1 are mutated in autosomal-recessive Pitt-Hopkins-like mental retardation and determine the level of a common synaptic protein in Drosophila. *Am. J. Hum. Genet.* **85**, 655–666 (2009).

5. Arking, D. E., Cutler, D. J., Brune, C. W., Teslovich, T. M., West, K., Ikeda, M., Rea, A., Guy, M., Lin, S., Cook, E. H. & Chakravarti, A. A common genetic variant in the neurexin superfamily member CNTNAP2 increases familial risk of autism. *Am. J. Hum. Genet.* **82**, 160–164 (2008).

6. Anney, R., Klei, L., Pinto, D., Almeida, J., Bacchelli, E., Baird, G., Bolshakova, N., Bölte, S., Bolton, P. F., Bourgeron, T., Brennan, S., Brian, J., Casey, J., Conroy, J., Correia, C., Corsello, C., Crawford, E. L., de Jonge, M., Delorme, R., Duketis, E., Duque, F., Estes, A., Farrar, P., Fernandez, B. A., Folstein, S. E., Fombonne, E., Gilbert, J., Gillberg, C., Glessner, J. T., Green, A., Green, J., Guter, S. J., Heron, E. A., Holt, R., Howe, J. L., Hughes, G., Hus, V., Igliozzi, R., Jacob, S., Kenny, G. P., Kim, C., Kolevzon, A., Kustanovich, V., Lajonchere, C. M., Lamb, J.

A., Law-Smith, M., Leboyer, M., Le Couteur, A., Leventhal, B. L., Liu, X.-Q., Lombard, F., Lord, C., Lotspeich, L., Lund, S. C., Magalhaes, T. R., Mantoulan, C., McDougle, C. J., Melhem, N. M., Merikangas, A., Minshew, N. J., Mirza, G. K., Munson, J., Noakes, C., Nygren, G., Papanikolaou, K., Pagnamenta, A. T., Parrini, B., Paton, T., Pickles, A., Posey, D. J., Poustka, F., Ragoussis, J., Regan, R., Roberts, W., Roeder, K., Roge, B., Rutter, M. L., Schlitt, S., Shah, N., Sheffield, V. C., Soorya, L., Sousa, I., Stoppioni, V., Sykes, N., Tancredi, R., Thompson, A. P., Thomson, S., Tryfon, A., Tsiantis, J., Van Engeland, H., Vincent, J. B., Volkmar, F., Vorstman, J. a. S., Wallace, S., Wing, K., Wittemeyer, K., Wood, S., Zurawiecki, D., Zwaigenbaum, L., Bailey, A. J., Battaglia, A., Cantor, R. M., Coon, H., Cuccaro, M. L., Dawson, G., Ennis, S., Freitag, C. M., Geschwind, D. H., Haines, J. L., Klauck, S. M., McMahon, W. M., Maestrini, E., Miller, J., Monaco, A. P., Nelson, S. F., Nurnberger, J. I., Oliveira, G., Parr, J. R., Pericak-Vance, M. A., Piven, J., Schellenberg, G. D., Scherer, S. W., Vicente, A. M., Wassink, T. H., Wijsman, E. M., Betancur, C., Buxbaum, J. D., Cook, E. H., Gallagher, L., Gill, M., Hallmayer, J., Paterson, A. D., Sutcliffe, J. S., Szatmari, P., Vieland, V. J., Hakonarson, H. & Devlin, B. Individual common variants exert weak effects on the risk for autism spectrum disorders. *Hum. Mol. Genet.* **21**, 4781–4792 (2012).

7. de la Torre-Ubieta, L., Won, H., Stein, J. L. & Geschwind, D. H. Advancing the understanding of autism disease mechanisms through genetics. *Nat. Med.* **22**, 345–361 (2016).

8. Parikshak, N. N., Gandal, M. J. & Geschwind, D. H. Systems biology and gene networks in neurodevelopmental and neurodegenerative disorders. *Nat. Rev. Genet.* **16**, 441–458 (2015).

9. Schafer, S. T., Paquola, A. C. M., Stern, S., Gosselin, D., Ku, M., Pena, M., Kuret, T. J. M., Liyanage, M., Mansour, A. A., Jaeger, B. N., Marchetto, M. C., Glass, C. K., Mertens, J. & Gage, F. H. Pathological priming causes developmental gene network heterochronicity in autism patient-derived neurons. *Nat. Neurosci.* **22**, 243–255 (2019).

10. Poot, M. Connecting the CNTNAP2 Networks with Neurodevelopmental Disorders. *Mol. Syndromol.* **6**, 7–22 (2015).

11. Poliak, S., Gollan, L., Martinez, R., Custer, A., Einheber, S., Salzer, J. L., Trimmer, J. S., Shrager, P. & Peles, E. Caspr2, a new member of the neurexin superfamily, is localized at the juxtaparanodes of myelinated axons and associates with K+ channels. *Neuron* **24**, 1037–1047 (1999).

12. Anderson, G. R., Galfin, T., Xu, W., Aoto, J., Malenka, R. C. & Südhof, T. C. Candidate autism gene screen identifies critical role for cell-adhesion molecule CASPR2 in dendritic arborization and spine development. *Proc. Natl. Acad. Sci.* **109**, 18120–18125 (2012).

13. Peñagarikano, O., Abrahams, B. S., Herman, E. I., Winden, K. D., Gdalyahu, A., Dong, H., Sonnenblick, L. I., Gruver, R., Almajano, J., Bragin, A., Golshani, P., Trachtenberg, J. T., Peles, E. & Geschwind, D. H. Absence of CNTNAP2 Leads to Epilepsy, Neuronal Migration Abnormalities, and Core Autism-Related Deficits. *Cell* **147**, 235–246 (2011).

14. Liska, A., Bertero, A., Gomolka, R., Sabbioni, M., Galbusera, A., Barsotti, N., Panzeri, S., Scattoni, M. L., Pasqualetti, M. & Gozzi, A. Homozygous Loss of Autism-Risk Gene CNTNAP2 Results in Reduced Local and Long-Range Prefrontal Functional Connectivity. *Cereb. Cortex* **28**, 1141–1153 (2018).

15. Panza, P., Sitko, A. A., Maischein, H.-M., Koch, I., Flötenmeyer, M., Wright, G. J., Mandai, K., Mason, C. A. & Söllner, C. The LRR receptor Islr2 is required for retinal axon routing at the vertebrate optic chiasm. *Neural Develop.* **10**, (2015).

16. Abudureyimu, S., Asai, N., Enomoto, A., Weng, L., Kobayashi, H., Wang, X., Chen, C., Mii, S. & Takahashi, M. Essential Role of Linx/Islr2 in the Development of the Forebrain Anterior Commissure. *Sci. Rep.* **8**, 7292 (2018).

17. Mandai, K., Reimert, D. V. & Ginty, D. D. Linx Mediates Interaxonal Interactions and Formation of the Internal Capsule. *Neuron* **83**, 93–103 (2014).

18. Alarcón, M., Abrahams, B. S., Stone, J. L., Duvall, J. A., Perederiy, J. V., Bomar, J. M., Sebat, J., Wigler, M., Martin, C. L., Ledbetter, D. H., Nelson, S. F., Cantor, R. M. & Geschwind, D. H. Linkage, Association, and Gene-Expression Analyses Identify CNTNAP2 as an Autism-Susceptibility Gene. *Am. J. Hum. Genet.* **82**, 150–159 (2008).

19. Lancaster, M. A., Renner, M., Martin, C.-A., Wenzel, D., Bicknell, L. S., Hurles, M. E., Homfray, T., Penninger, J. M., Jackson, A. P. & Knoblich, J. A. Cerebral organoids model human brain development and microcephaly. *Nature* **501**, 373–379 (2013).

20. Chambers, S. M., Fasano, C. A., Papapetrou, E. P., Tomishima, M., Sadelain, M. & Studer, L. Highly efficient neural conversion of human ES and iPS cells by dual inhibition of SMAD signaling. *Nat. Biotechnol.* **27**, 275–280 (2009).
21. Kim, E. J., Jacobs, M. W., Ito-Cole, T. & Callaway, E. M. Improved Monosynaptic Neural Circuit Tracing Using Engineered Rabies Virus Glycoproteins. *Cell Rep.* **15**, 692–699 (2016).
22. Network inefficiencies in autism spectrum disorder at 24 months. - PubMed - NCBI. https://www.ncbi.nlm.nih.gov/pubmed/24802306.
23. MBF Bioscience. Neurolucida. https://www.mbfbioscience.com/neurolucida.

24. Berg, S., Kutra, D., Kroeger, T., Straehle, C. N., Kausler, B. X., Haubold, C., Schiegg, M., Ales, J., Beier, T., Rudy, M., Eren, K., Cervantes, J. I., Xu, B., Beuttenmueller, F., Wolny, A., Zhang, C., Koethe, U., Hamprecht, F. A. & Kreshuk, A. ilastik: interactive machine learning for (bio)image analysis. *Nat. Methods* **16**, 1226–1232 (2019).

25. O'Reilly, C., Lewis, J. D. & Elsabbagh, M. Is functional brain connectivity atypical in autism? A systematic review of EEG and MEG studies. *PloS One* **12**, e0175870 (2017).

26. Dennis, E. L., Jahanshad, N., Rudie, J. D., Brown, J. A., Johnson, K., McMahon, K. L., de Zubicaray, G. I., Montgomery, G., Martin, N. G., Wright, M. J.,

Bookheimer, S. Y., Dapretto, M., Toga, A. W. & Thompson, P. M. Altered Structural Brain Connectivity in Healthy Carriers of the Autism Risk Gene, CNTNAP2. *Brain Connect.* **1**, 447–459 (2011).

27. Varea, O., Martin-de-Saavedra, M. D., Kopeikina, K. J., Schürmann, B., Fleming, H. J., Fawcett-Patel, J. M., Bach, A., Jang, S., Peles, E., Kim, E. & Penzes, P. Synaptic abnormalities and cytoplasmic glutamate receptor aggregates in contactin associated protein-like 2/Caspr2 knockout neurons. *Proc. Natl. Acad. Sci.* **112**, 6176–6181 (2015).

28. Qian, X., Nguyen, H. N., Song, M. M., Hadiono, C., Ogden, S. C., Hammack, C., Yao, B., Hamersky, G. R., Jacob, F., Zhong, C., Yoon, K., Jeang, W., Lin, L., Li, Y., Thakor, J., Berg, D. A., Zhang, C., Kang, E., Chickering, M., Nauen, D., Ho, C.-Y., Wen, Z., Christian, K. M., Shi, P.-Y., Maher, B. J., Wu, H., Jin, P., Tang, H., Song, H. & Ming, G. Brain-Region-Specific Organoids Using Mini-bioreactors for Modeling ZIKV Exposure. *Cell* **165**, 1238–1254 (2016).

29. B Hughes, R., Whittingham-Dowd, J., Simmons, R. E., Clapcote, S. J., Broughton, S. J. & Dawson, N. Ketamine Restores Thalamic-Prefrontal Cortex Functional Connectivity in a Mouse Model of Neurodevelopmental Disorder-Associated 2p16.3 Deletion. *Cereb. Cortex* doi:10.1093/cercor/bhz244.

30. Lecciso, F. & Colombo, B. Beyond the Cortico-Centric Models of Cognition: The Role of Subcortical Functioning in Neurodevelopmental Disorders. *Front. Psychol.* **10**, (2019).

31. Micheva, K. D. & Phend, K. D. Conjugate Immunofluorescence—SEM Array Tomography for Studying Mammalian Synapses and Axons. in *Cellular Imaging: Electron Tomography and Related Techniques* (ed. Hanssen, E.) 149–182 (Springer International Publishing, 2017). doi:10.1007/978-3-319-68997-5_6.

32. The RNAi Consortium. *Broad Institute* https://www.broadinstitute.org/scientific-community/science/projects/rnai-consortium/rnai-consortium (2008).

33. ZEISS ZEN Microscope Software for Microscope Components. https://www.zeiss.com/microscopy/us/products/microscope-software/zen.html.

34. Schindelin, J., Arganda-Carreras, I., Frise, E., Kaynig, V., Longair, M., Pietzsch, T., Preibisch, S., Rueden, C., Saalfeld, S., Schmid, B., Tinevez, J.-Y., White, D. J., Hartenstein, V., Eliceiri, K., Tomancak, P. & Cardona, A. Fiji: an open-source platform for biological-image analysis. *Nat. Methods* **9**, 676–682 (2012).